

Ultimate Acceleration in Quantum Mechanics to Explain and Calculate Earth's Geomagnetic Field: 0.6Gauss

Huaiyang Cui

Department of Physics, Beihang University, Beijing, 102206, China

Email: hycui@buaa.edu.cn

(October 28, 2022, submitted to viXra; March 9, 2023, revised)

Abstract: In analogy with the ultimate speed c , there is an ultimate acceleration β , nobody's acceleration can exceed this limit β , in the solar system, $\beta=2.961520e+10(\text{m/s}^2)$. Because this ultimate acceleration is large, any effect related to β will become easy to test, including quantum gravity tests. In this paper, an approach is put forward to connect the ultimate acceleration with quantum theory, and is applied to sunspot, earth's tropic cyclones, and earth's geomagnetic field problems. The sunspot cycle is calculated to be 10.93 years due to the ultimate acceleration. A simulation was carried out, clearly showing the inner structure of a cyclone, which is consistent with the famous DIANA cyclone on 12 September 1984 in situ observation measured by an aircraft. The sunspot structure is also investigated, which has a similarity to that of a tropic cyclone. The ultimate acceleration provides a mechanism to explain geomagnetic field, the earth's geomagnetic field is calculated to be 0.6Gauss at the north pole.

1. Introduction

In general, some quantum gravity proposals [1,2] are extremely hard to test in practice, as quantum gravitational effects are appreciable only at the Planck scale [3]. But ultimate acceleration provides another method to deal with quantum gravity effects.

In analogy with the ultimate speed c , there is an ultimate acceleration β , nobody's acceleration can exceed this limit β , in the solar system, $\beta=2.961520e+10(\text{m/s}^2)$. Because this ultimate acceleration is large, any effect related to β will become easy to test, including quantum gravity tests. In this paper, an approach is put forward to connect the ultimate acceleration with quantum theory, and is applied to sunspot, earth's tropic cyclones, and earth's geomagnetic field problems.

2. How to connect the ultimate acceleration with quantum theory

In relativity, the speed of light c is the ultimate speed, nobody's speed can exceed this limit c . The relativistic velocity u of a particle in the coordinate system $(x_1, x_2, x_3, x_4=ict)$ satisfies

$$u_1^2 + u_2^2 + u_3^2 + u_4^2 = -c^2 . \quad (1)$$

No matter what particles (electrons, molecules, neutrons, quarks), their 4-vector velocities all have the same magnitude: $|u|=ic$. All particles gain **equality** because of the same magnitude of the 4-velocity u . The acceleration a of a particle is given by

$$a_1^2 + a_2^2 + a_3^2 = a^2; \quad (a_4 = 0; \quad \because x_4 = ict) \quad (2)$$

Assume that particles have an ultimate acceleration β as the limit, no particle can exceed this acceleration limit β . Subtracting both sides of the above equation by β^2 , we have

$$a_1^2 + a_2^2 + a_3^2 - \beta^2 = a^2 - \beta^2; \quad a_4 = 0 \quad (3)$$

It can be rewritten as

$$[a_1^2 + a_2^2 + a_3^2 + 0 + (i\beta)^2] \frac{1}{1 - a^2 / \beta^2} = -\beta^2 \quad (4)$$

Now, the particle has an acceleration whose five components are specified by

$$\begin{aligned} \alpha_1 &= \frac{a_1}{\sqrt{1 - a^2 / \beta^2}}; & \alpha_2 &= \frac{a_2}{\sqrt{1 - a^2 / \beta^2}}; \\ \alpha_3 &= \frac{a_3}{\sqrt{1 - a^2 / \beta^2}}; & \alpha_4 &= 0; & \alpha_5 &= \frac{i\beta}{\sqrt{1 - a^2 / \beta^2}}; \end{aligned} \quad (5)$$

where α_5 is the newly defined acceleration in five-dimensional space-time $(x_1, x_2, x_3, x_4=ict, x_5)$. Thus, we have

$$\alpha_1^2 + \alpha_2^2 + \alpha_3^2 + \alpha_4^2 + \alpha_5^2 = -\beta^2; \quad \alpha_4 = 0 \quad (6)$$

It means that the magnitude of the newly defined acceleration α for every particle takes the same value: $|\alpha|=i\beta$ (constant imaginary number), all particle accelerations gain **equality** for the sake of the same magnitude.

How do resolve the velocity u and acceleration α into x , y , and z components? In a realistic world, a hand can rotate a ball moving around a circular path at constant speed v with constant centripetal acceleration a , as shown in Fig.1(a). Likewise, the u and α let the particle move spirally, as shown in Fig.1(b), projecting out the real x , y , and z components.

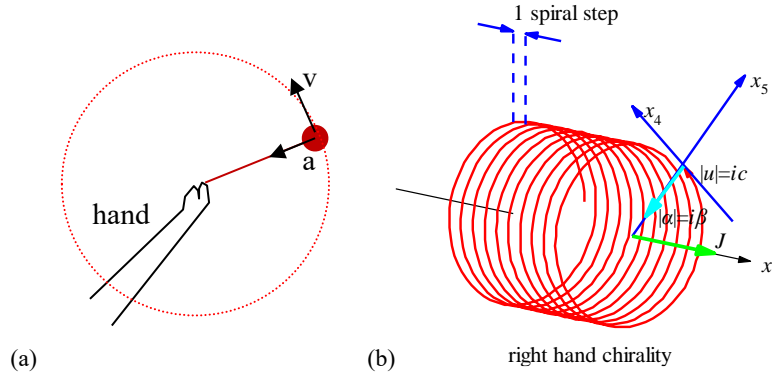


Fig.1 (a) A hand rotates a ball moving around a circular path at constant speed v with constant centripetal acceleration a . (b) The particle moves along the x_1 axis with the constant speed $|u|=ic$ in u direction and constant centripetal force in the x_5 axis at the radius iR (imaginary number).

```
<Clet2020 Script>/[26]
double D[100],S[2000];int i,j,R,X,N;
int main(){R=50;X=50;N=600;D[0]=-50;D[1]=0;D[2]=0;D[3]=X;D[4]=0;D[5]=0;D[6]=-50;D[7]=R;D[8]=0;
D[9]=600;D[10]=10;D[11]=R;D[12]=0;D[13]=3645;
Lattice(SPIRAL,D,S);SetViewAngle(0,80,-50);DrawFrame(FRAME_NULL,1,0xfffff);
Draw("LINE,0,2,XYZ,0","-150,0,0,-50,0,0");Draw("ARROW,0,2,XYZ,10","50,0,0,150,0,0");
SetPen(2,0xffff0000);Plot("POLYLINE,0,600,XYZ",S[9]);i=9+3*N-6;Draw("ARROW,0,2,XYZ,10",S[i]);
TextHang(S[i],S[i+1],S[i+2]," #if|u|=ic#t");TextHang(150,0,0," #ifx#sd1#t");SetPen(2,0x005fff);
Draw("LINE,1,2,XYZ,8","-50,0,50,-50,0,100");Draw("LINE,1,2,XYZ,8","-40,0,50,-40,0,100");
Draw("ARROW,0,2,XYZ,10","-80,0,100,-50,0,100");Draw("ARROW,0,2,XYZ,10","-10,0,100,-40,0,100");
TextHang(-50,0,110,"1 spiral step");i=9+3*N;S[i]=50;S[i+1]=10;S[i+2]=10;
```

```

Draw("ARROW,0,2,XYZ,10","50,0,0,50,80,80");TextHang(50,80,80," #ifx#sd5#t");
Draw("ARROW,0,2,XYZ,10","50,72,0,50,0,72");TextHang(50,0,72," #ifx#sd4#t");
SetPen(3,0x00ffff);Draw("ARROW,0,2,XYZ,15",S[i-3]);TextHang(S[i],S[i+1],S[i+2]," #ifl#alpha=i#beta#t");
SetPen(3,0x00ff00);Draw("ARROW,0,2,XYZ,15","50,0,0,120,0,0");TextHang(110,5,5," #ifl#t");
TextHang(-60,0,-80," right hand chirality");}#v07=?>A#t

```

In analogy with the ball in a circular path, consider a particle in one-dimensional motion along the x_1 axis at the speed v , in Fig.1(b) it moves with the constant speed $|u|=ic$ almost along the x_4 axis and slightly along the x_1 axis, and the constant centripetal acceleration $|\alpha|=i\beta$ in the x_5 axis at the constant radius iR (imaginary number); the coordinate system $(x_1, x_4=ict, x_5=iR)$ establishes a cylinder coordinate system in which this particle moves spirally at the speed v along the x_1 axis. According to the usual centripetal acceleration formula $a=v^2/r$, the acceleration in the x_4 - x_5 plane is given by

$$a = \frac{v^2}{r} \Rightarrow i\beta = \frac{|u|^2}{iR} = -\frac{c^2}{iR} = i\frac{c^2}{R} . \quad (7)$$

Therefore, the track of the particle in the cylinder coordinate system $(x_1, x_4=ict, x_5=iR)$ forms a shape, called **acceleration-roll**. The faster the particle moves along the x_1 axis, the longer the spiral step is.

Like a steel spring that contains an elastic wave, the track in the acceleration-roll in Fig.1(b) can be described by a wave function whose phase changes 2π for one spiral step. Apparently, **this wave is just the de Broglie's matter wave for electrons, protons or quarks, etc.**

Theorem: the acceleration-roll bears matter wave.

$$\psi = \exp\left(i\frac{\beta}{c^3} \int_0^x (u_1 dx_1 + u_2 dx_2 + u_3 dx_3 + u_4 dx_4)\right) . \quad (8)$$

Proof: See ref. [28,30].

Depending on the particle under investigation, this wave function may have different explanations. If the β is replaced by the Planck constant, the wave function of electrons is given by

$$\begin{aligned} \text{assume: } \beta &= \frac{mc^3}{\hbar} \\ \psi &= \exp\left(\frac{i}{\hbar} \int_0^x (mu_1 dx_1 + mu_2 dx_2 + mu_3 dx_3 + mu_4 dx_4)\right) \end{aligned} \quad (9)$$

where $mu_4 dx_4 = -Edt$, it strongly suggests that the wave function is just the de Broglie's matter wave [4,5,6].

Considering another explanation to ψ for planets in the solar system, no Planck constant can be involved. But, in a many-body system with the total mass M , the data analysis [28] tells us that the ultimate acceleration can be rewritten in terms of **Planck-constant-like constant h** as

$$\begin{aligned} \text{assume: } \beta &= \frac{c^3}{hM} \\ \psi &= \exp\left(\frac{i}{hM} \int_0^x (u_1 dx_1 + u_2 dx_2 + u_3 dx_3 + u_4 dx_4)\right) \end{aligned} \quad (10)$$

The constant h will be determined by experimental observations. This paper will show that this wave function is applicable to several many-body systems in the solar system, the wave function is called the **acceleration-roll wave**.

Tip: actually, ones cannot get to see the acceleration-roll of a particle in the relativistic space-time $(x_1, x_2, x_3, x_4 = ict)$; only get to see it in the cylinder coordinate system $(x_1, x_4 = ict, x_5 = iR)$.

3. How to determine the ultimate acceleration

In Bohr's orbit model for planets or satellites, as shown in Fig.2, the circular quantization condition is given in terms of relativistic matter wave in gravity by

$$\left. \begin{aligned} \frac{\beta}{c^3} \oint_L v_l dl = 2\pi n \\ v_l = \sqrt{\frac{GM}{r}} \end{aligned} \right\} \Rightarrow \sqrt{r} = \frac{c^3}{\beta \sqrt{GM}} n; \quad n = 0, 1, 2, \dots \quad (11)$$

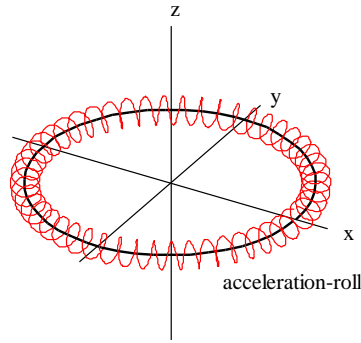


Fig.2 A planet 2D orbit around the sun, an acceleration-roll winding around the planet.

```
<Clet2020 Script>[[26]
int i,j,k; double r,rot,x,y,z,D[20],F[20],S[200]; int main(){SetViewAngle("temp0,theta60,phi-30");
DrawFrame(FRAME LINE,1,0xaffaf);r=80;Spiral(); TextHang(r,-r,0,"acceleration-roll");
r=110;TextHang(r,0,0,"x");TextHang(0,r,0,"y");TextHang(0,0,r,"z");}
Spiral(){r=80;j=10;rot=j/r;k=2*PI/rot+1;
for(i=0;i<k;i+=1){D[0]=x;D[1]=y;D[2]=z;D[6]=x;D[7]=y;D[8]=r;
x=r*cos(rot*i);y=r*sin(rot*i);z=0;if(i==0) continue;
SetPen(2,0x00);F[0]=D[0];F[1]=D[1];F[2]=x;F[3]=y;Draw("LINE,0,2,XY","F");SetPen(1,0xff0000);
D[3]=x;D[4]=y;D[5]=z; D[9]=40;D[10]=10;D[11]=8;D[12]=0;D[13]=360;
Lattice(SPIRAL,D,S);Plot("POLYLINE,0,40,XYZ",S[9]);}
}#v07=?>A#
```

The solar system, Jupiter's satellites, Saturn's satellites, Uranus' satellites, and Neptune's satellites as five different many-body systems are investigated with the Bohr's orbit model. After fitting observational data as shown in Fig.3, their ultimate accelerations are obtained in Table 1. The predicted quantization blue-lines in Fig.3(a), Fig.3(b), Fig.3(c), Fig.3(d) and Fig.3(e) agree well with experimental observations for those *inner constituent planets or satellites*.

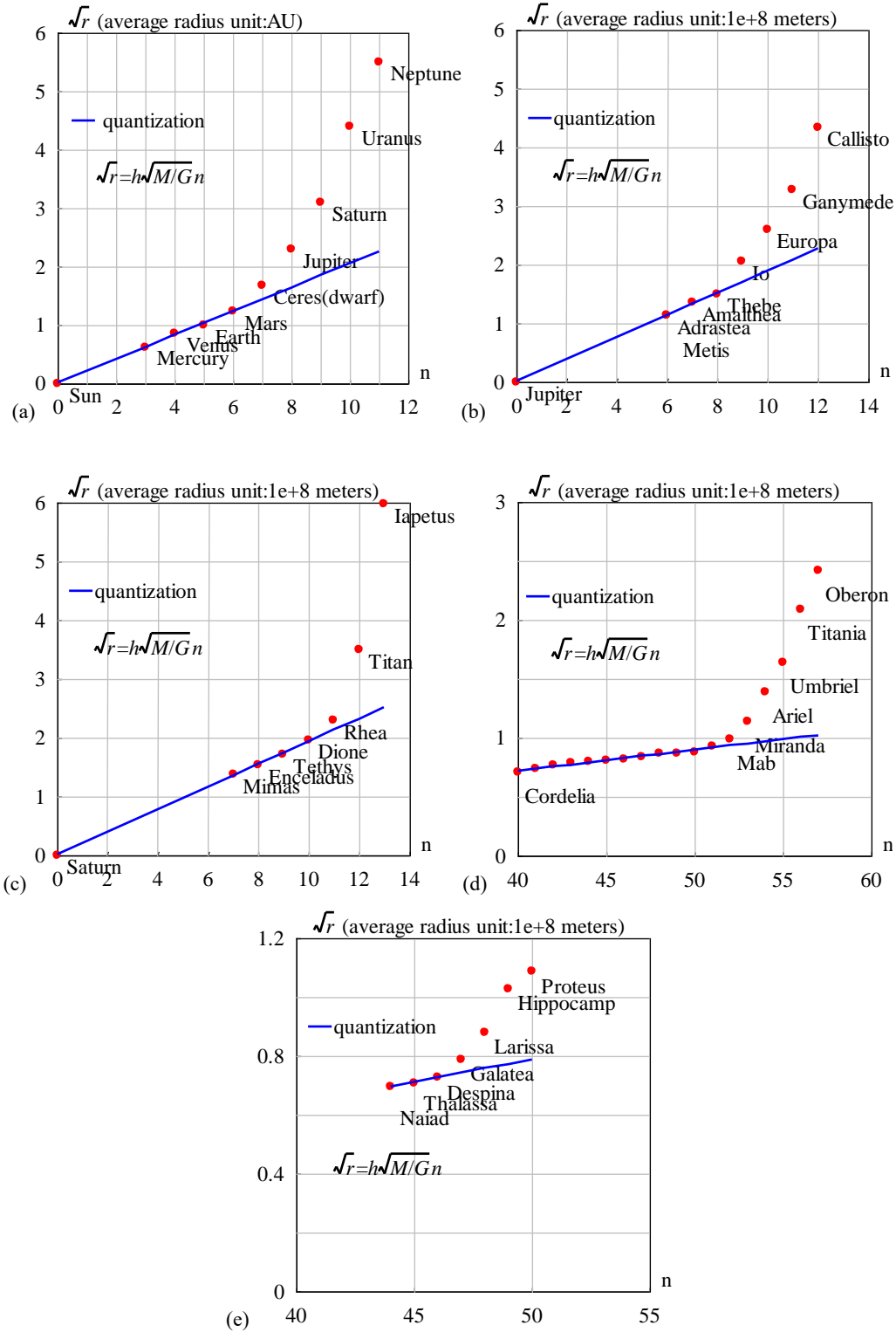


Fig.3 The orbital radii are quantized for inner constituents. (a) the solar system with $h=4.574635e-16$ ($m^2s^{-1}kg^{-1}$). The relative error is less than 3.9%. (b) the Jupiter system with $h=3.531903e-16$ ($m^2s^{-1}kg^{-1}$). Metis and Adrastea are assigned the same quantum number for their almost same radius. The relative error is less than 1.9%. (c) the Saturn system with $h=6.610920e-16$ ($m^2s^{-1}kg^{-1}$). The relative error is less than 1.1%. (d) the Uranus system with $h=1.567124e-16$ ($m^2s^{-1}kg^{-1}$). $n=0$ is assigned to Uranus. The relative error is less than 2.5%. (e) the Neptune system with $h=1.277170e-16$ ($m^2s^{-1}kg^{-1}$). $n=0$ is assigned to Neptune. The relative error is less than 0.17%.

Table 1 Planck-constant-like constant h , N is constituent particle number with smaller orbital inclination.

system	N	M/M_{earth}	β (m/s ²)	h (m ² s-1kg-1)	Prediction
Solar planets	9	333000	2.961520e+10	4.574635e-16	Fig.3(a)
Jupiter' satellites	7	318	4.016793e+13	3.531903e-16	Fig.3(b)
Saturn's satellites	7	95	7.183397e+13	6.610920e-16	Fig.3(c)
Uranus' satellites	18	14.5	1.985382e+15	1.567124e-16	Fig.3(d)
Neptune 's satellites	7	17	2.077868e+15	1.277170e-16	Fig.3(e)

Besides every β , our interest shifts to the constant h in Table 1, which is defined as

$$h = \frac{c^3}{M\beta} \Rightarrow \sqrt{r} = h\sqrt{\frac{M}{G}}n \quad (12)$$

In a many-body system with a total mass of M , a constituent particle has the mass of m and moves at the speed of v , it is easy to find that the wavelength of de Broglie's matter wave should be modified for planets and satellites as

$$\lambda_{de_Broglie} = \frac{2\pi\hbar}{mv} \Rightarrow \text{modify} \Rightarrow \lambda = \frac{2\pi hM}{v} \quad (13)$$

where h is a **Planck-constant-like constant**. Usually, the total mass M is approximately equal to the central-star's mass. It is found that this modified matter wave works for quantizing orbits correctly in Fig.3 [28,29]. The key point is that the various systems have almost the same Planck-constant-like constant h in Table 1 with a mean value of $3.51\text{e-}16 \text{ m}^2\text{s}^{-1}\text{kg}^{-1}$, at least having the same magnitude! The acceleration-roll wave is a generalized matter wave on a planetary scale.

In Fig.3(a), the blue straight line expresses the linear regression relation among the Sun, Mercury, Venus, Earth and Mars, their quantization parameters are $hM=9.098031\text{e+}14(\text{m}^2/\text{s})$. The ultimate acceleration is fitted out to be $\beta=2.961520\text{e+}10 \text{ (m/s}^2\text{)}$. Where, $n=3,4,5,\dots$ were assigned to solar planets, the sun was assigned a quantum number $n=0$ because the sun is in the **central state**.

4. Optical model of the central state

The acceleration-roll wave as the relativistic matter wave generalized in gravity is given by

$$\psi = \exp\left(\frac{i}{hM} \int_0^x v_l dl\right); \quad \lambda = \frac{2\pi hM}{v_l} = \frac{2\pi c^3}{v_l \beta} \quad (14)$$

In a central state $n=0$, if the coherent length of the acceleration-roll wave is long enough, its head may overlap with its tail when the particle moves in a closed orbit in space-time, as shown in Fig.4, the interference of the acceleration-roll wave between its head and tail will occur in the overlapping zone. The overlapped wave is given by

$$\psi(r) = 1 + e^{i\delta} + e^{i2\delta} + \dots + e^{i(N-1)\delta} = \frac{1 - \exp(iN\delta)}{1 - \exp(i\delta)} \quad (15)$$

$$\delta(r) = \frac{1}{hM} \oint_L (v_l) dl = \frac{2\pi\omega r^2}{hM} = \frac{2\pi\beta\omega r^2}{c^3}$$

where N is the overlapping number which is determined by the coherent length of the acceleration-roll wave, δ is the phase difference after one orbital motion, ω is the angular speed of the solar rotation. The above equation is a multi-slit interference formula in optics, for a larger N it is called the Fabry-Perot interference formula.

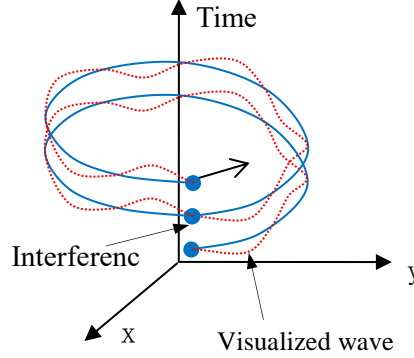


Fig.4 The head of the acceleration-roll wave may overlap with its tail.

The acceleration-roll wave function ψ needs a further explanation. In quantum mechanics, $|\psi|^2$ equals to the probability of finding an electron due to Max Burn's explanation; in astrophysics, $|\psi|^2$ equals to the probability of finding a nucleon (proton or neutron) *averagely on an astronomic scale*, because all mass is mainly made of nucleons, we have

$$|\psi|^2 \propto \text{nucleon_density} \quad (16)$$

It follows from the multi-slit interference formula that the interference intensity at maxima is proportional to N^2 , that is

$$N^2 = \frac{|\psi(0)_{\text{multi-wavelet}}|^2}{|\psi(0)_{\text{one-wavelet}}|^2} \quad (17)$$

What matter plays the role of “one-wavelet” in the solar core or earth core? We choose air-vapor at the sea level on the earth's surface as the “reference matter: one-wavelet”. Thus, the overlapping number N is estimated by

$$N^2 = \frac{|\psi(0)_{\text{multi-wavelet}}|^2}{|\psi(0)_{\text{one-wavelet}}|^2} \approx \frac{\text{core_nucleon_density}_{r=0}}{\text{air_vapor_density}_{r=sea}} \quad (18)$$

Although today there is no air-vapor on the solar surface, does not hinder to select it as the reference matter. The solar core has a maximum density of $1.5e+5\text{kg/m}^3$ [31], comparing to the air-vapor density of 1.29 kg/m^3 at the sea level on the earth, the solar overlapping number N is estimated as $N=341$. The earth's core density is $5.53e+3\text{kg/m}^3$, the earth's overlapping number N is estimated as $N=65$.

For the Sun, Earth and Mars, their central densities and their reference matter density are

given in Table 2. Thus, their overlapping numbers are estimated also in this table.

Sun's angular speed at the equator is known as $\omega=2\pi/(25.05*24*3600)$, unit: s^{-1} . Its mass $1.9891e+30$ (kg), radius $6.95e+8$ (m), mean density 1408 (kg/m^3), the solar core has a maximum density of $1.5e+5kg/m^3$ [31], the ultimate acceleration $\beta=2.961520e+10$ (m/s^2), the constant $hM=9.100745e+14$ (m^2/s). According to the $N=341$, the matter distribution of the $|\psi|^2$ is calculated in Fig.5, it agrees well with the general description of the sun's interior. The radius of the sun is calculated to be $r=7e+8$ (m) with a relative error of 0.72% in Fig.5, which indicates that the sun radius strongly depends on the sun's self-rotation.

Table 2 Estimating the overlapping number N by comparing solid core to reference matter, regarding protons and neutrons as basis particles.

object	Solid core, density (kg/m^3)	Reference matter, density (kg/m^3)	Overlapping number N	β (m/s^2)
Sun	$1.5e+5$ (max.)	1.29 (vapor above the sea)	341	$2.961520e+10$
Earth	5530	1.29 (vapor above the sea)	65	$1.377075e+14$
Mars	3933.5	1.29 (vapor above the sea)	55	$2.581555e+15$
Jupiter	1326			$4.016793e+13$
Saturn	687			$7.183397e+13$
Uranus	1270			$1.985382e+15$
Neptune	1638			$2.077868e+15$
Alien-planet	5500	1.29(has water on the surface)	65	

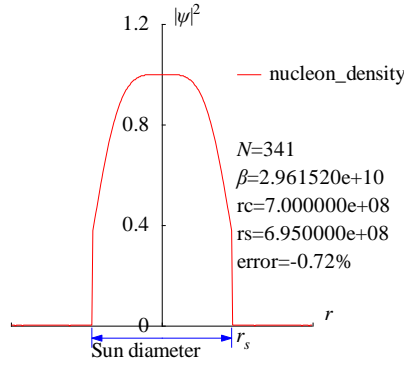


Fig.5 The matter distribution $|\psi|^2$ around the Sun has been calculated in the radius direction.

```
<Clet2020 Script>[/[26]
int i,j,k,m,n,N,nP[10];
double beta,H,B,M,r,r_unit,x,y,z,delta,D[1000],S[1000], a,b,rs,rc,rot,atm_height; char str[100];
main(){k=150;rs=6.95e8;rc=0;x=25.05;rot=2*PI/(x*24*3600);n=0; N=341;
beta=2.961520e10;H=SPEEDC*SPEEDC*SPEEDC/beta;M=1.9891E30; atm_height=2e6; r_unit=1E7;
b=PI(2*PI*rot*rs*rs/H);
for(i=-k;i<k;i+=1){r=abs(i)*r_unit;
if(r<rs+atm_height) delta=2*PI*rot*r/H; else delta=2*PI*sqrt(GRAVITYC*M*r)/H;//around the star
y=SumJob("SLIT_ADD,@N,@delta",D); y=y/(N*N);
S[n]=i;S[n+1]=y; if(i>0 && rc==0 && y<0.001) rc=r;D[n]=i;D[n+1]=z;n+=2;}
SetAxis(X_AXIS,-k,0,k,"#ifr; ;");SetAxis(Y_AXIS,0,0,1.2,"#ifpsi#su2#;0;0.4;0.8;1.2;");
DrawFrame(FRAME_SCALE,1,0xaffaf); z=100*(rs-rc)/rs;
SetPen(1,0xff0000);Polyline(k+k,S,k/2,1," nucleon_density"); SetPen(1,0x0000ff); //Polyline(k+k,D);
//Draw("LINE,0,2,XY,0","20,0.5,60,0.6");TextHang(60,0.6,0,"core");
r=rs/r_unit;y=-0.05;D[0]=-r;D[1]=y;D[2]=r;D[3]=y; Draw("ARROW,3,2,XY,10,100,10,10,");D);
Format(str,"#ifN#t=%d#n#ifbeta#t=%e#nrc=%e#nrs=%e#nerror=%0.2f%",N,beta,rc,rs,z);
TextHang(k/2,0.7,0,str);TextHang(r+5,y/2,0,"#if#sds#");TextHang(-r,y+0,"Sun diameter");
}#v07=?>A#t
```


$$v_i = \sqrt{\frac{GM}{r}}; \quad \delta(r) = \frac{1}{hM} \oint_L (v_i) dl = \frac{\beta}{c^3} \oint_L (v_i) dl = \frac{2\pi\beta}{c^3} \sqrt{GMr} \quad (20)$$

The secondary peaks over the atmosphere up to 2000km altitude are calculated in Fig.7(b) which agree well with the space debris observations [16]; the peak near 890 km altitude is due principally to the January 2007 intentional destruction of the FengYun-1C weather spacecraft, while the peak centered at approximately 770 km altitude was created by the February 2009 accidental collision of Iridium 33 (active) and Cosmos 2251 (derelict) communication spacecraft [16,18]. The observations based on the incoherent scattering radar EISCAT ESR located at 78°N in Jul. 2006 and in Oct. 2015 [21,22,23] are respectively shown in Fig.7(c) and (d). This prediction of secondary peaks also agrees well with other space debris observations [24,25].

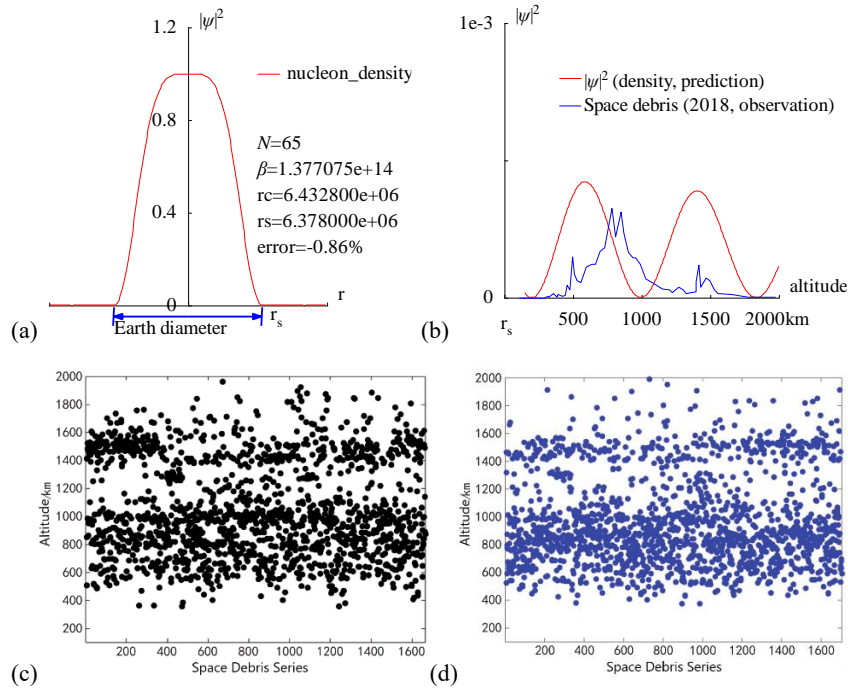


Fig.7 (a) The radius of the Earth is calculated out $r=6.4328e+6$ (m) with a relative error of 0.86% by the interference of its acceleration-roll wave; (b) The prediction of the space debris distribution up to 2000km altitude; (c) The space debris distribution in Jul. 2006, Joint observation based on the incoherent scattering radar EISCAT ESR located at 78°N [21]; (d) The space debris distribution in Oct. 2015, Joint observation based on the incoherent scattering radar EISCAT ESR located at 78°N [21].

```
<Clet2020 Script>/[26]
int i,j,k,m,n,N,nP[10]; double H,B,M,v_r,r,AU,r_unit,x,y,z,delta,D[10],S[1000];
double rs,rc,rot,a,b,atm_height,beta; char str[100];
main(){k=80;rs=6.378e6;rc=0;atm_height=1.5e5;n=0; N=65;
beta=1.377075e+14;H=SPEEDC*SPEEDC*SPEEDC/beta;
M=5.97237e24;AU=1.496E11;r_unit=1e-6*AU; rot=2*PI/(24*60*60);/angular speed of the Earth
for(i=-k;i<k;i+=1){r=abs(i)*r_unit;
if(r<rs+atm_height) v_r=rot*r**r; else v_r=sqrt(GRAVITYC*M*r);/around the Earth
delta=2*PI*v_r/H; y=SumJob("SLIT_ADD,@N,@delta",D); y=y/(N*N);
if(y>1) y=1; S[n]=i;S[n+1]=y; if(i>0 && rc=0 && y<0.001) rc=r; n+=2;}
SetAxis(X_AXIS,-k,0,k,"r"; ; );SetAxis(Y_AXIS,0,0,1.2,"#if\psi/#su2#t;0;0.4;0.8;1.2;");
DrawFrame(FRAME_SCALE,1,0,xa,ffa); x=50;z=100*(rs-rc)/rs;
SetPen(1,0,ffa);Polyline(k+k,S,k/2,1," nucleon density");
r=rs/r_unit;y=-0.05;D[0]=-r;D[1]=y;D[2]=r;D[3]=y;
SetPen(2,0,ffa); Draw("ARROW,3,2,XY,10,100,10,10,"D);
Format(str,"#ifN#=#d#n#ifB#t=#e#nrc=#e#nrs=#e#nerror=#.2f%",N,beta,rc,rs,z);
TextHang(k/2,0.7,0,str);TextHang(r+5,y/2,0,"r#sds#t");TextHang(-r,y+0,"Earth diameter");
}#v07=?>A#t
```

```

<Clet2020 Script>//[26]
int i,j,k,m,n,N,nP[10]; double H,B,M,v_r,r,AU,r_unit,x,y,z,delta,D[10],S[10000];
double rs,rc,rot,a,b,atm_height,p,T,R1,R2,R3; char str[100]; int
Debris[96]={110,0,237,0,287,0,317,2,320,1,357,5,380,1,387,4,420,2,440,3,454,14,474,9,497,45,507,26,527,19,557,17,597,34,63
4,37,664,37,697,51,727,55,781,98,808,67,851,94,871,71,901,50,938,44,958,44,991,37,1028,21,1078,17,1148,10,1202,9,1225,6,
1268,12,1302,9,1325,5,1395,7,1395,18,1415,36,1429,12,1469,22,1499,19,1529,9,1559,5,1656,4,1779,1,1976,1,};
main(){k=80;rs=6.378e6;rc=0;atm_height=1.5e5;n=0;N=65;
H=1.956611e11;M=5.97237e24;AU=1.496E11;r_unit=1e4;
rot=2*PI/(24*60*60);//angular speed of the Earth
b=PI/(2*PI*rot*rs*rs/H); R1=rs/r_unit;R2=(rs+atm_height)/r_unit;R3=(rs+2e6)/r_unit;
for(i=R2;i<R3;i+=1) {r=abs(i)*r_unit; delta=2*PI*sqrt(GRAVITYC*M*r)/H;
y=SumJob("SLIT_ADD,@N,@delta",D); y=1e3*y/(N*N);// visualization scale:1000
if(y>1) y=1; S[n]=i;S[n+1]=y;n+=2;}
SetAxis(X_AXIS,R1,R1,R3,"altitude; r#sds#:500;1000;1500;2000km ");
SetAxis(Y_AXIS,0,0,1,"#if|#su2#:0; ;1e-3;");DrawFrame(FRAME_SCALE,1,0,xaffaf); x=R1+(R3-R1)/5;
SetPen(1,0xff0000);Polyline(n/2,S,x,0.8,"#if|#su2# (density, prediction)");
for(i=0;i<48;i+=1) {S[i+i]=R1+(R3-R1)*Debris[i+i]/2000; S[i+i+1]=Debris[i+i+1]/300;}
SetPen(1,0x0000ff);Polyline(48,S,x,0.7,"Space debris (2018, observation) "); }#v07=?>A#

```

6. Sunspot cycle

The **coherence length** of waves is usually mentioned but the **coherence width** of waves is rarely discussed in quantum mechanics, simply because the latter is not a matter for electrons, nucleon, or photons, but it is a matter in astrophysics. The analysis of observation data tells us that on the planetary scale, the coherence width of acceleration roll waves can be extended to 1000 kilometers or more, as illustrated in Fig.8(a), the overlap may even occur in the width direction, thereby bringing new aspects to wave interference.

In the solar convective zone, adjacent convective arrays form a top-layer flow, a middle-layer gas, and a ground-layer flow, similar to the concept of **molecular current** in electromagnetism. Considering one convective ring at the equator as shown in Fig.8(b), there is an apparent velocity difference between the top-layer flow and the middle-layer gas, where their acceleration-roll waves are denoted respectively by

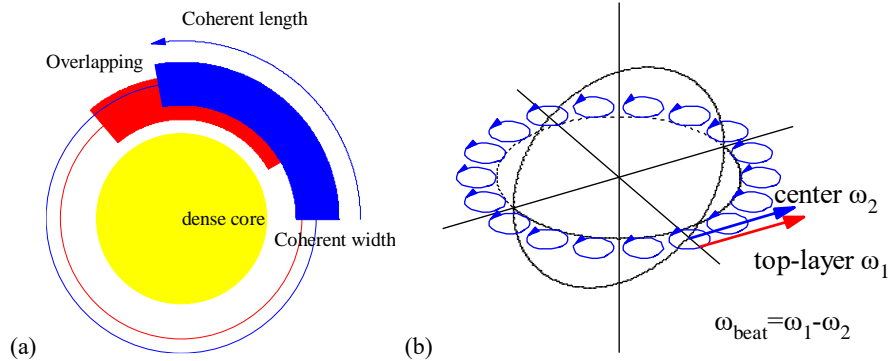


Fig.8 (a) Illustration of overlapping in the coherent width direction. (b) In convective rings at the equator, the speed difference causes a beat frequency.

```

<Clet2020 Script> [26]
int i, j, k, R, D[500];
main(){DrawFrame(FRAME_NULL,1,0,xaffaf);
R=60; SetPen(1,0xffff00);
D[0]=-R; D[1]=-R; D[2]=R; D[3]=R; Draw("ELLIPSE,1,2,XY,0",D);
R=85; k=15; SetPen(1,0xff0000);
D[0]=-R; D[1]=-R; D[2]=R; D[3]=R; Draw("ELLIPSE,0,2,XY,0",D);
D[0]=0; D[1]=0; D[2]=R-k; D[3]=0; D[4]=R+k;D[5]=0;
Draw("SECTOR,1,3,XY,15,30,130,0",D);
R=95; k=15; SetPen(1,0x00ff);
D[0]=-R; D[1]=-R; D[2]=R; D[3]=R; Draw("ELLIPSE,0,2,XY,0",D);
D[0]=0; D[1]=0; D[2]=R-k; D[3]=0; D[4]=R+k;D[5]=0;
Draw("SECTOR,1,3,XY,15,0,100,0",D);D[4]=R+k+k;
Draw("SECTOR,3,3,XY,15,0,100,0",D);
TextHang(0,0,0,"dense core");TextHang(R-k-k,-k,0,"Coherent width");
TextHang(0,R+k+k+k,0,"Coherent length");TextHang(-R,R+k,0,"Overlapping");
}#v07=?>A#

```

```

<Clet2020 Script>//Clet is a C compiler[26]
double beta,H,M,N,dP[20],D[2000],r,rs,rot,x,y,v1,v2,K1,K2,T1,T2,T,Lamda,L; int i,j,k;
int main() {beta=2.961520e10; H=SPEEDC*SPEEDC*SPEEDC/beta;
M=1.9891E30; rs=6.95e8;rot=2*PI/(25.05*24*3600);v1=rot*rs;K1=v1*v1/2;//T1=2*PI*H/K1;
v2=6100;//0.7346*sqrt(BOLTZMANN*5700/MP)+0.2485*sqrt(BOLTZMANN*5700/(MP+MP));
K2=v2*v2/2;T2=2*PI*H/(K2-K1);T=T2/24*3600*365.2422;
Lamda=2*PI*H/(v2-v1);L=2*PI*rs/Lamda;
SetViewAngle("temp0,theta60,phi-60");
DrawFrame(FRAME LINE,1,0xafffaf);Overlook("2,1,60", D);
TextAt(10,10,"v1=%d, v2=%d, T=%2f y, #n λ=%e, L=%d",v1,v2,T, Lamda,L);
SetPen(1,0x4f4fff); for(i=0;i<18;i+=1) {v1=i*2*PI/18; x=70*cos(v1);y=70*sin(v1);Ring();}
SetPen(2,0xff0000);Draw("ARROW,0,2,XYZ,15", "80,0,0,80,60,0");
TextHang(100,20,0,"top-layer ω#sd1#t"); SetPen(2,0x0000ff);
Draw("ARROW,0,2,XYZ,15", "70,0,0,70,60,0");
TextHang(50,60,0,"center ω#sd2#t");TextHang(140,-30,0," ω#sdbeat#t=ω#sd1#t-ω#sd2#t");
}
Ring(){ k=0;N=20; r=10;
for(j=0;j<N+2;j+=1) {k=j+j+j; v2=j*2*PI/N;
D[k]=x+r*cos(v2);D[k+1]=y+r*sin(v2); D[k+2]=0;}
Plot("POLYLINE,4,22,XYZ,8",D);}
#v07=?>A

```

$$\begin{aligned}
\psi &= \psi_{top} + C\psi_{middle} \\
\psi_{top} &= \exp\left[\frac{i\beta}{c^3} \int_L (v_1 dl + \frac{-c^2}{\sqrt{1-v_1^2/c^2}} dt)\right] \\
\psi_{middle} &= \exp\left[\frac{i\beta}{c^3} \int_L (v_2 dl + \frac{-c^2}{\sqrt{1-v_2^2/c^2}} dt)\right]
\end{aligned} \quad (21)$$

Their interference in the coherent width direction leads to a beat phenomenon

$$\begin{aligned}
|\psi|^2 &= |\psi_{top} + C\psi_{middle}|^2 = 1 + C^2 + 2C \cos\left[\frac{2\pi}{\lambda_{beat}} \int_L dl - \frac{2\pi}{T_{beat}} t\right] \\
\frac{2\pi}{T_{beat}} &= \frac{\beta}{c^3} \left(\frac{c^2}{\sqrt{1-v_1^2/c^2}} - \frac{c^2}{\sqrt{1-v_2^2/c^2}} \right) \approx \frac{\beta}{c^3} \left(\frac{v_1^2}{2} - \frac{v_2^2}{2} \right) \\
\frac{2\pi}{\lambda_{beat}} &= \frac{\beta}{c^3} (v_1 - v_2); \quad V = \frac{\lambda_{beat}}{T_{beat}} = \frac{1}{2} (v_1 + v_2)
\end{aligned} \quad (22)$$

Their speeds are calculated as

$$\begin{aligned}
v_1 &\approx 6200 \text{ (m/s)} \quad (\approx \text{observed in Evershed flow}) \\
v_2 &= \omega r_{middle} = 2017 \text{ (m/s)} \quad (\text{solar rotation});
\end{aligned} \quad (23)$$

Where, regarding Evershed flow as the eruption of the top-layer flow, about 6km/s speed was reported [31]. Alternatively, the top-layer speed v_1 also can be calculated in terms of thermodynamics, to be $v_1=6244$ (m/s) [28]. Here using $v_1=6100$ (m/s), their beat period T_{beat} is calculated to be a very remarkable value of 10.93 (years), in agreement with the sunspot cycle value (say, mean 11 years).

$$T_{beat} \approx \frac{4\pi c^3}{\beta(v_1^2 - v_2^2)} = 10.93 \text{ (years)} \quad (24)$$

The relative error to the mean 11 years is 0.6% for the beat period calculation using the acceleration-roll waves. This beat phenomenon turns out to be a **nucleon density oscillation** that undergoes to drive the sunspot cycle evolution. The beat wavelength λ_{beat} is too long to observe, only the beat period is easy to be observed. As shown in Fig.9, on the solar surface, the equatorial circumference $2\pi r$ only occupies a little part of the beat wavelength, what we see is

the expansion and contraction of the nucleon density.

$$\frac{2\pi r}{\lambda_{beat}} = 0.0031 \quad (25)$$

This nucleon density oscillation is understood as a new type of nuclear reaction on an astronomic scale.

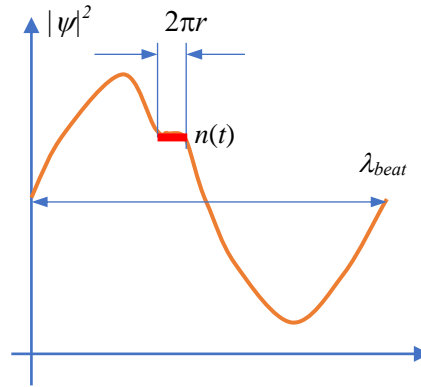


Fig.9 The equatorial circumference $2\pi r$ only occupies a little part of the beat wavelength, what we see is the expansion and contraction of the nucleon density.

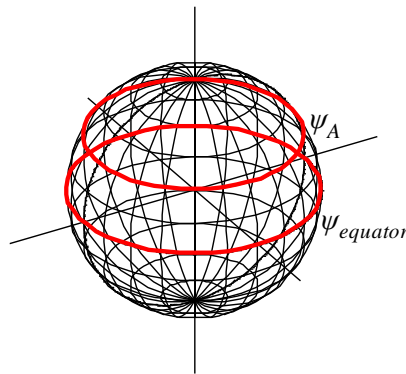
In the above calculation, although this seems to be a rough model, there is an obvious correlation between solar radius, solar rotation, solar density, ultimate acceleration, and Planck-constant-like constant h .

7. Atmospheric circulation

Consider an acceleration-roll wave ψ_A in the earth shell at the latitude angle A , it will interfere with its neighbor waves within its coherent width. Because the earth shell mainly consists of dense matter, their mutual cascade-interference will cause the acceleration roll wave to have the same phase at the same longitude, so that the acceleration roll wave ψ_A should equal to the $\psi_{equator}$ at the same longitude, as shown in Fig.10(a). This conclusion is supported by the spherical symmetry of the Earth's density distribution, that is.

$$\text{spherical symmetry: } \rho(r, A, \varphi) = \rho(r) \Rightarrow \psi(r, A, \varphi) = \psi(r) \quad (26)$$

$$\text{or: } \psi_A = \psi_{equator}$$



(a)



(b)

Fig.10 (a) Mutual cascade-interference will lead to the acceleration-roll wave having the same phase. (b) Jupiter

(the photo from News).

```
<Clet2020 Script> [26]
double dP[20],D[2000], r, v1,v2,K1,K2; int i,j,k,N;
int main(){SetViewAngle("temp0,theta60,phi-60");
DrawFrame(FRAME_LINE,1,0xafffaf);Overlook("2,1,60", D);
for(i=0;i<180;i+=15){k=0; K1=0; K2=i;Grid();}
for(i=0;i<180;i+=15){k=1; K1=i; K2=0;Grid();}
SetPen(3,0xff0000); k=1; K1=60; K2=0;Grid();K1=90; K2=0; Grid();
//SetPen(3,0x4f4fff); k=1; K1=55; K2=0;Grid();K1=65; K2=0; Grid();
TextHang(40,40,50,"#ifψ#sdA#"); TextHang(50,40,0,"#ifψ#sdequator#t");
}
Grid();{N=50; K1*=PI/180; K2*=PI/180; r=60;
if(k==0){v1=2*PI/N; v2=0;} else {v1=0; v2=2*PI/N;}
for(j=0;j<=N;j+=1){ k=j+j;
D[k]=r*sin(K1)*cos(K2);D[k+1]=r*sin(K1)*sin(K2); D[k+2]=r*cos(K1);
K1+=v1;K2+=v2; }Plot("POLYGON,0,50, XYZ,10",D);
}#v07=?>A#t
```

On the contrary, in the thin atmosphere, the cascade-interference within the coherence width can be ignored, so the wind and clouds are widely distributed in the sky on a large scale.

Through the coherent width concept, considering the interference between the air ψ_A at the latitude angle A and the shell ψ_{shell} at the same latitude, they are

$$\begin{aligned} \psi(r, A) &= \psi_{air}(r, A) + C\psi_{shell}(r, A) = \psi_{air}(r, A) + C\psi_{shell_equator}(r) \\ T_{beat} &\simeq \frac{4\pi c^3}{\beta(v_{shell_equator}^2 - v_{air}^2)} \quad . \quad (27) \\ v_{shell_equator} &= \omega r \\ v_{air} &= \omega r \cos(A) + v_{wind} + v_{sun_effect} \end{aligned}$$

where C represents the coupling constant which relates to their distance and mass fractions, their interference leads to a beat phenomenon. The positive wind denotes the direction from west to east. The air is subjected to the solar radiation which enforces the beat oscillation to run at the period $T_{beat}=1$ (year) at the latitude angles $A=-23.5^\circ N \sim 23.5^\circ N$ due to the tilt of the earth axis concerning the earth orbital plane. We have known that there is a beat $T_{beat}=1$ year in the first constructive interference ridge with zero wind at the latitude A_1 , using the above neat period formula we obtain the sun effect:

$$v_{sun_effect} = 369.788 - \omega r \cos(A_1); \quad (units : m / s) \quad . \quad (28)$$

It is not easy to maintain the constructive interference condition for these waves. When the first ridge is at latitude $A_1=12^\circ N$, the wind required for maintaining the beat $T_{beat}=1$ (year) near the latitude $A=12^\circ N$ is calculated as shown in Fig.11(a) (blue line), this wind will be destroyed by destructive interference at higher latitudes. But, the wind will arise up again at the next locations where the waves satisfy the constructive interference condition: at $A=50^\circ N$ location where beat $T_{beat}=0.5$ (years), and at $A=70^\circ N$ location where beat $T_{beat}=0.37$ (years) which is the shortest period that the earth can get within the arctic regions. The maximal wind appears most probably at the midst of the first two ridges, about 48m/s. Linking all characteristic points in Fig.11(a) we obtain the predicted wind-curve over the northern hemisphere; this prediction agrees well with the experimental observations at an altitude of 10km (200hPa), as shown in Fig.12.

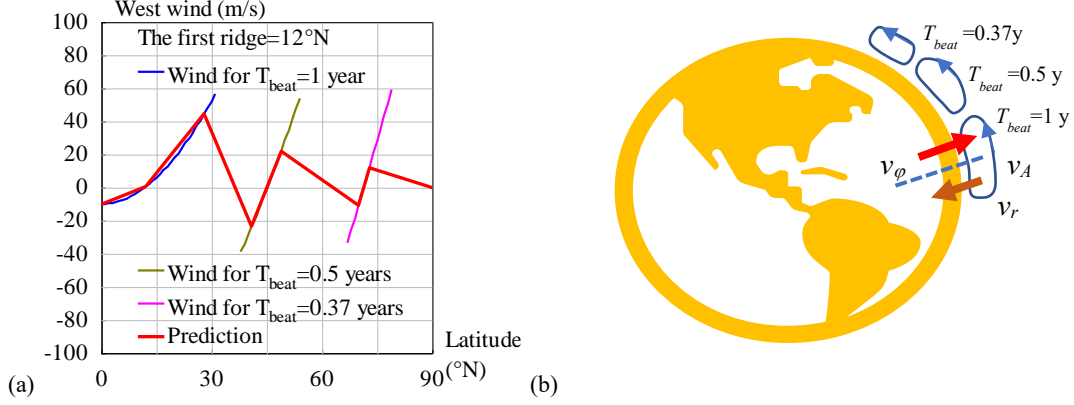


Fig.11 (a) Calculation of west winds in the northern hemisphere. (b) The atmospheric circulation in the northern hemisphere.

```

<Clet2020 Script> [26]
double beta,H,M,r,rc, rs, rot,v1,v2, Year,T,Lamda,V,a,b,w,Fmax,N[500],S[500],F[100]; int i, j, k, t, m, n, s, f,Type,x;
int main(){beta=1.377075e+14; H=SPEEDC*SPEEDC*SPEEDC/beta;
M=5.97237e24; rs=6.371e6; rot=2*PI/(24*3600); Year=24*3600*365.2422;
Type=1; x=10; if(Type>1) x=-30;
if(Type==1) SetAxis(X_AXIS,0,0,90,"Latitude#n(°N);0;30;60;90;");
else SetAxis(X_AXIS,-90,-90,90,"Latitude#n(°N);=90;-60;-30;0;30;60;90;");
SetAxis(Y_AXIS,-100,-100,100,"West wind (m/s);-100;-80;-60;-40;-20;0;20;40;60;80;100;");
DrawFrame(0x016a,Type,0xaffaf);//Polyline(2,"-90,0,90,0");
Check(15,k); if(k>24) k=24; if(k<0) k=0;
T=Year/2; Wind(); f=0; Findf(); t=N[m+m]; T=Year; Wind(); f=0; Findf();
SetPen(2,0xff); Polyline(n,N,x,70,"Wind for T#sdbeat#t=1 year"); if(Type>1) Polyline(s,S);
F[0]=N[0];F[1]=N[1]; F[2]=N[m+m]; F[3]=N[m+m+1]; t=(t+F[2])/2;//midst of two ridges
t=t-F[2]+m; Fmax=N[t+t+1]; //TextAt(100,20,"t=%d, Fmax=%f",t,Fmax);
f=Fmax; Findf(); F[4]=N[m+m]; F[5]=N[m+m+1];
T=Year/2; Wind(); f=-Fmax/2; Findf(); t=m;f=-Fmax/2; Findf();
SetPen(2,0x80ff00); Polyline(n,N,x,-50,"Wind for T#sdbeat#t=0.5 years"); if(Type>1) Polyline(s,S);
F[6]=N[t+t]; F[7]=N[t+t+1]; F[8]=N[m+m]; F[9]=N[m+m+1];
T=0.37*Year; Wind(); f=-Fmax/4; Findf(); t=m;f=-Fmax/4; Findf();
SetPen(2,0x9933fa); Polyline(n,N,x,-70,"Wind for T#sdbeat#t=0.37 years"); if(Type>1) Polyline(s,S);
F[10]=N[t+t]; F[11]=N[t+t+1]; F[12]=N[m+m]; F[13]=N[m+m+1]; F[14]=90; F[15]=0;
SetPen(3,0xff0000); Polyline(8,F,x,-90,"Prediction");
TextHang(x,90,0,"The first ridge=%d°N", k);
}
Wind(){n=0;s=0;
for(i=0;i<90;i+=1) { a=i*PI/180; v1=rot*rs*cos(a); v2=rot*rs;
w=369.788-v2*cos(k*PI/180); a=v2*v2-4*PI*H/T; V=sqrt(a)-v1-w;
if(V>-40 && V<60) {N[n+n]=i; N[n+n+1]=V; n+=1;}}
for(i=0;i<90;i+=1) { a=-i*PI/180;v1=rot*rs*cos(a); v2=rot*rs;
w=369.788-v2*cos(k*PI/180); a=v2*v2-4*PI*H/T; V=sqrt(a)-v1-w;
if(V>-40 && V<60) {S[s+s]=-i; S[s+s+1]=V; s+=1;}}
Findf(){a=1e10; for(i=0;i<n;i+=1) { b=N[i+1]-f;if(b<0) b=-b;if(b<a) {m=i;a=b;}}
}
#v07=?>A

```

For further improvement of precision, the value of the wind required by the constructive interference condition should be understood as a magnitude, it should be resolved into three components in the spherical coordinates (r, A, φ) as

$$v_{wind}^2 = v_r^2 + v_A^2 + v_\varphi^2 \quad (29)$$

According to the energy equipartition theorem in thermodynamics, approximately we have the average estimation

$$\langle v_r^2 \rangle = \langle v_A^2 \rangle = \langle v_\varphi^2 \rangle = \frac{1}{3} v_{wind}^2 \quad (30)$$

Thus, the wind vectors around the northern hemisphere of the Earth are plotted in Fig.11(b), the atmospheric circulation consists of three cells: Hadley cell, Ferrel cell, and arctic cell.

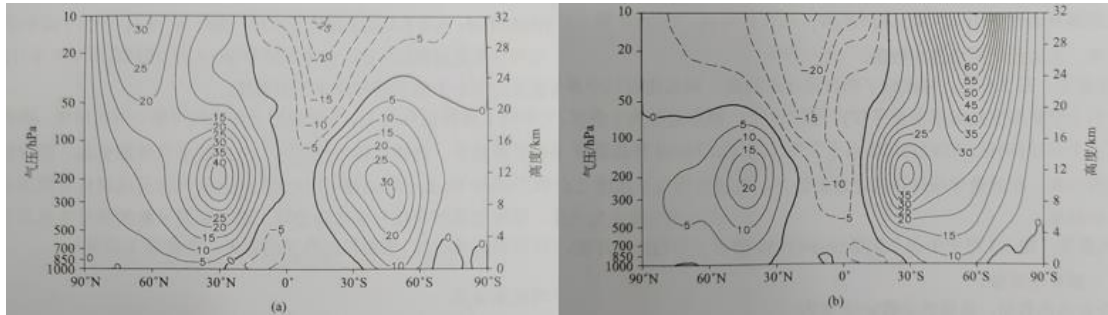


Fig.12 NCEP/NCAR data, mean west winds over 40 years (1958~1997) [36]. (a) in winter; (b) in summer.

The beat $T_{beat}=0.5$ (years) blows comfortable winds over Europe, Northern America and Northeastern Asia, and modulates the four seasons; the shortest beat $T_{beat}=0.37$ (years) has a beat wavelength too long to be confined in the arctic regions so that it escapes from the north pole toward the equator, so recognized as the planet-scale waves or Rossby waves.

Since the acceleration-roll wave of the air interferes with the acceleration-roll wave of the equatorial shell, the easterlies at the equator have a magnitude of about 10 m/s. The trade winds or easterlies are the permanent east-to-west prevailing winds that flow in the Earth's equatorial region. The trade winds blow mainly from the northeast in the Northern Hemisphere and the southeast in the Southern Hemisphere, strengthening during the winter and when the Arctic oscillation is in its warm phase. Trade winds have been used by captains of sailing ships to cross the world's oceans for centuries. The driving force of atmospheric circulation is the uneven distribution of solar heating across the earth, which is greatest near the equator and least at the poles. This air rises to the tropopause, about 10–15 kilometers above sea level, where the air is no longer buoyant [33].

Consider a funny issue, as we have known that $v_{sun_effect}=-84$ (m/s) at the equator when the first ridge at $A_1=12^\circ\text{N}$, imagine if nuclear wars happen on the Earth to stop the solar radiation to the Earth's surface, then the equatorial wind on the Earth's surface will simply reach to 94 (m/s), like the winds on the surfaces of the Jupiter and Saturn [28], this will change global climate mode, killed all dinosaurs by strong winds and dusts. Thinking about Mars, Jupiter, and Saturn that gain very weak solar radiation, and there are at least 100 (m/s) strong winds on their surfaces, as shown in Fig.10(b). It tells us how important is the easterly 10 (m/s) at the equator for us, and how important is the air pollution for us. Have you ever gotten an experience: [the more serious the air pollution, the stronger the wind?](#) This section helps us understand how the dinosaurs to be buried.

8. Inner structure of tropical cyclones

A tropical cyclone is a rapidly rotating storm system characterized by a low-pressure center, a closed low-level atmospheric circulation, strong winds, and a spiral arrangement of thunderstorms that produce heavy rain and squalls. Tropical cyclones on either side of the Equator generally have their origins in several tropical cyclone basins, as shown in Fig.13. The Northwest Pacific Ocean is the most active basin on the planet, accounting for one-third of all tropical cyclone activity. Warm sea surface temperatures are required for tropical cyclones to form and strengthen. The commonly-accepted minimum temperature range for this to occur is

26–27 °C [37,38].

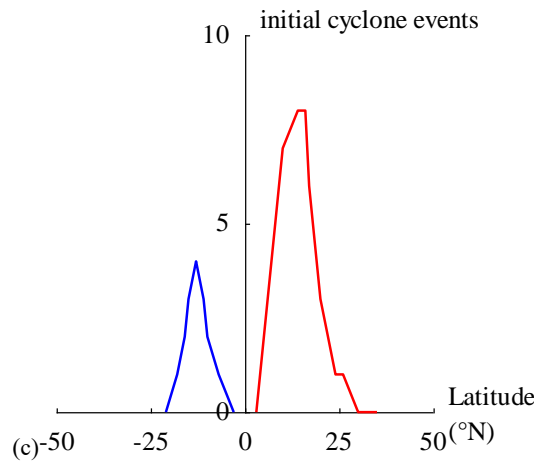


Fig.13 Initial tropical cyclone events in the northern sphere and southern sphere.[35]

The latitude $A=12^{\circ}\text{N}$ is called the **first constructive interference ridge** sandwiched between easterlies and westerlies, where the shear action of the winds will produce a lot of vortexes if the winds are disturbed by vapors at higher altitudes. The pregnancy of a tropical cyclone needs three steps, as shown in Fig.14(a).

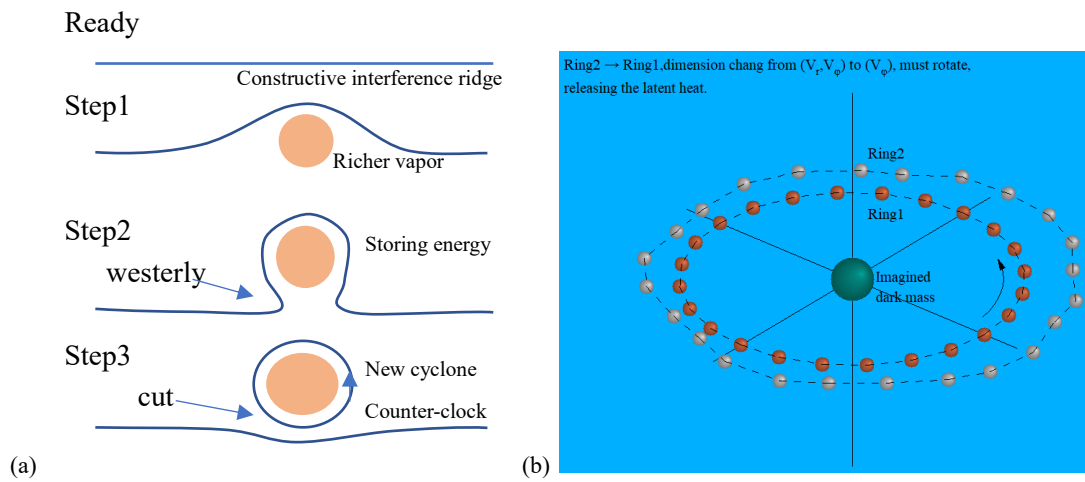


Fig.14 (a)Three steps of the pregnancy of a tropic cyclone in the northern hemisphere. (b) Dimension change on a molecular scale.

```
<Clet2020 Script>// [26]
double r,x,y,z,v, a,b,c,dP[20],D[500]; int i,j,k ;
main(){ SetViewAngle("temp0.theta60,phi-40"); DrawFrame(FRAME_LINE,2,0xafff);
dP[0]=PEARL; dP[1]=0xefeefe; dP[2]=1; dP[3]=XYZ;
dP[4]=10; dP[5]=10; dP[6]=0; dP[7]=50; dP[8]=30; dP[9]=30;
r=100; b=10; j=0;
for(i=0;i<360;i+=15) { a=i*PI/180; x=r*cos(a); y=r*sin(a); z=0;
x+=b*random(); y+=b*random();
D[j+j+j]=x; D[j+j+j+1]=y; D[j+j+j+2]=z; Plot(dP,D[j+j+j]); j+=1; }
Plot("POLYGON,1,@j,XYZ,10,",D);
r=80; b=6; dP[1]=0xff7f50; j=0;
for(i=0;i<360;i+=15) { a=i*PI/180; x=r*cos(a); y=r*sin(a); z=0;
D[j+j+j]=x; D[j+j+j+1]=y; D[j+j+j+2]=z; Plot(dP,D[j+j+j]); j+=1; }
Plot("POLYGON,1,@j,XYZ,10,",D);
TextHang(10,0,70,"Ring2#n#n#nRing1");
TextAt(100,200,"Ring2 → Ring1,dimension chang from (V#sd#t,V#sdφ#t) to (V#sdφ#t), must rotate,#nreleasing the latent heat.");
D[0]=0; D[1]=0; D[2]=0; dP[1]=0x03a89e; dP[4]=30; dP[5]=30; Plot(dP,D);
TextHang(8,8,0,"Imagined #ndark mass"); r=70; j=0;
for(i=10;i<60;i+=5) { a=i*PI/180; x=r*cos(a); y=r*sin(a); z=0;
D[j+j+j]=x; D[j+j+j+1]=y; D[j+j+j+2]=z; j+=1; }
dP[0]=POLYLINE; dP[1]=3; dP[2]=j; dP[3]=XYZ; dP[4]=15; Plot(dP,D);
```

}
#v07=?>A#t

Step1, during summer, the richer vapor at higher altitudes over the warm sea surface dramatically absorbs the solar radiation and releases the $v_{sun_effect} = -85(m/s)$ into the air at lower altitudes; consequently, the strengthened easterlies make a distortion to the first constructive interference ridge, as shown in Fig.14(a).

Step2, day by day, the distortion develops to an extent that it is going to separate from the mother-like first constructive interference ridge hit strongly by the westerlies, as shown in Fig.14(a).

Step3, finally, the distorted constructive interference ridge grows up to become an isolated baby ring which is recognized as a new tropical cyclone, counter-clockwise in the northern hemisphere, as shown in Fig.14(a), similar to Fig.10(b) there is a large vortex on the surface of Jupiter.

The pregnancy of tropical cyclones tends to develop at the latitude $A=12^\circ N$, it is a relativistic quantum mechanical effect that cannot be solved by classical fluid mechanics. Recalling that the latitude $A=12^\circ N$ represents the mean latitude angle which is subjected to the main solar radiation activity in the northern hemisphere, actually, the solar radiation varies its mostly shined latitudes within the range of $A=-23.5^\circ N \sim 23.5^\circ N$ due to the tilt of the earth axis concerning the earth orbital plan, therefore actual pregnancy latitude of tropical cyclones occur among latitude angles $A=-23.5^\circ N \sim 23.5^\circ N$, this result agrees well with the experimental records.

In Fig.11(a), there are the second, the third, ..., constructive interference ridges to bear the pregnancy of cyclones, hurricanes, typhoons, storms, tornados. Without these flexible constructive interference ridges, it is difficult for classical physics to say that some disturbances would somehow support the persistence of the vortexes.

For understanding the pregnancy process on a molecular scale, considering there are two molecular rings in Fig.14(b), typically the air molecules move on the Earth's surface in 2D motion. From ring2 to ring1, there is a dimension change for the molecules whose velocity changes from (v_r, v_ϕ) to (v_ϕ) , from 2D to 1D, losing the r component velocity. According to the energy equipartition theorem, every molecule would lose its kinetic energy as the latent heat released into the sky as

$$E_{latent} = \frac{2}{2} kT - \frac{1}{2} kT = \frac{1}{2} kT \quad . \quad (31)$$

At this moment, the molecules have to rotate about the cyclone's center. Losing an amount of the molecular kinetic energy will lead to the ring1 to be in a stationary bound state, whose binding force and binding energy are given by

$$F_{centripetal} = -\frac{\Delta E}{\Delta r} = -\frac{N_{molecules} E_{latent}}{\Delta r} \quad . \quad (32)$$

$$E_{binding} = N_{molecules} E_{latent}$$

As you wish, you can say that at the cyclone's center there exists an **imagined dark mass** which contributes to this binding force by using the universal gravitational formula.

When the constructive interference ring of a newly born cyclone forms, its wavelength will adapt to the ring size as

$$\frac{1}{hM_{cyclone}} \oint_L v_l dl = 2\pi n; \quad n = 1, 2, \dots \quad (33)$$

$$\psi = \exp\left(\frac{i}{hM_{cyclone}} \int_0^x (u_1 dx_1 + u_2 dx_2 + u_3 dx_3 + u_4 dx_4)\right)$$

where the mass M represents the overall mass of the new cyclone, including the **imagined dark mass** which accounts for the latent heat released during its formation; the constant h is the **Planck-constant-like constant** determined by experimental observations. The air molecules of the ring are under the control of their acceleration-roll waves whose coherent length is so long that the waves have to overlap as

$$\psi(r) = 1 + e^{i\delta} + e^{i2\delta} + \dots + e^{i(N-1)\delta} = \frac{1 - \exp(iN\delta)}{1 - \exp(i\delta)} \quad (34)$$

$$\delta(r) = \frac{1}{hM_{cyclone}} \oint_L (v_l) dl$$

This formula can be used to calculate the distribution of the cyclone's nucleon density. In the preceding section on the central state optical model, we have mentioned that the air-vapor only concerns one wavelet interference, so that the overlapping number N of air-vapor of the cyclones simply takes 2, the structure of tropical cyclones becomes easier to calculate, that is

$$\psi(r) = 1 + e^{i\delta} = 1 + \cos(\delta) + i \sin(\delta) \quad (35)$$

It follows that the full expression is given in 2D cylinder wave form by

$$\psi(r)_{interference} = \sqrt{\frac{r_0}{r}} \sin(\delta) e^{i(k_r r - \omega t)} = \sqrt{\frac{r_0}{r}} \sin\left(\frac{v 2\pi r}{hM}\right) e^{i(k_r r - \omega t)} \quad (36)$$

On an altitude scale, a cyclone is divided into two layers: the upper layer and the lower layer. In the lower layer at the first ring the radius r_0 is proportional to the wavelength λ of the acceleration-roll wave, the swirling wind speed approximately is inversely proportional to radius r , and the maximal speed is about 45 (m/s) according to the theoretical prediction of the maximal wind in Fig.11(a) and the experimental observations in Fig.15(a), then

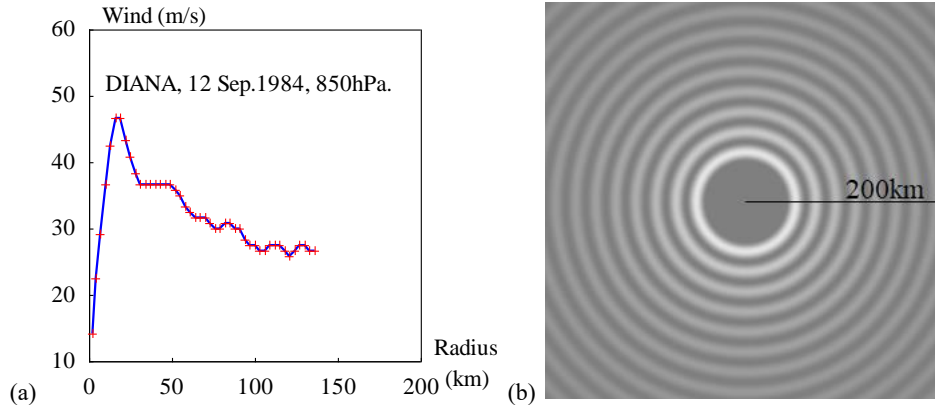


Fig.15 (a) Gradient wind as a function of the radius for the hurricane DIANA (12, Sep.1984) measured at 850hPa [40]. (b) The simulation of a cyclone using acceleration-roll wave, $|x| < 200$ km.

```
<Clet2020 Script>/[26]
int i,j,k,n; double x,y,nP[10];
int
D_Wind[92]={2,5,4,15,7,23,10,32,13,39,16,44,19,44,22,40,25,37,28,34,31,32,34,32,37,32,40,32,43,32,46,32,49,32,52,31,55,30,
58,28,61,27,64,26,67,26,70,26,73,25,76,24,79,24,82,25,85,25,88,24,91,24,94,22,97,21,100,21,103,20,106,20,109,21,112,21,115,
```

```

21,118,20,121,19,124,20,127,21,130,21,133,20,136,20,};
main(){SetAxis(X_AXIS,0,0,200,"Radius#n (km);0;50;100;150;200;");
SetAxis(Y_AXIS,0,0,60,"Wind (m/s); 10;20;30;40;50;60;");
DrawFrame(FRAME_BOX,1,0xaffaf);j=46;
SetPen(2,0xff); Polyline(j,D_Wind); SetPen(1,0xff0000);
nP[0]=CROSS;nP[1]=0;nP[2]=j;nP[3]=XY;nP[4]=4;nP[5]=4;Plot(nP,D_Wind);
TextHang(10,50,0,"DIANA, 12 Sep.1984, 850hPa.");
}#v07=?>A#t

```

```

<Clet2020 Script>/[26]
int i,j,k,nP[10]; double r_unit,Lamda,r,r0,r1,r2,v,v0,v1,w, a,b,delta, D[100];//1D array
main(){ w=150; r_unit=Te3;//km
r0=30*r_unit; r1=r0; Lamda=2*PI*r0; v0=15;v1=30;//m/s
DrawFrame(FRAME_NULL,1,0xaffaf); nP[0]=SET; nP[1]=1; nP[2]=PX;
for(i=-w;i<w;i+=1) { for(j=-w;j<w;j+=1) { r2=i*i+j*j;r=sqrt(r2)*r_unit;
if(r>r0) {b=r0/r; v=v0+v1*b; } else {b=0; v=v0*b;}
delta=2*PI*v*2*PI*r/(v0*Lamda);
a=sin(delta); a*=a; a*=b;//2D cylinder wave attenuation
nP[3]=Colorize(1,0xfffff.a);D[0]=250+i;D[1]=250+j;D[2]=0;PixelJob(nP,D); } }
Draw("LINE,0,2,XY,10","0,0,100,0");TextHang(50,5,0,"200km");
}#v07=?>A#t

```

$$2\pi r_0 = \lambda; \quad v_r = \frac{hM}{2\pi} k_r \quad . \quad (37)$$

$$r > r_0 : \quad v_\phi = v_0 + v_1 \frac{r_0}{r}; \quad v_0 = 15(m/s); \quad v_1 = 30(m/s)$$

A cyclone's acceleration-roll wave interference is simulated as shown in Fig.15(b), clearly showing the inner structure of a cyclone, well compared with the DIANA cyclone on 12 Sep. 1984 in situ observation measured by an aircraft [40]. Don't underestimate the profound role of the Planck-constant-like constant in cyclone structure; without it, all return to the classical fluid mechanics.

What is dark matter? Why it is important for cyclones and galaxies? Consider a galaxy whose gravity can captures any stars near the galaxy center by the universal gravitational force; the near field of the gravity can capture any star strolling in the galaxy's 2D plane and finally let this star move in a 1D circular orbit approximately, it makes a dimension change for the star from 2D to 1D with releasing latent heat. The far field of the gravity has to face stars strolling in 3D space, if it wants to capture these far stars, it must have an ability stronger than the universal gravitational force; in the far field, the gravitational force must become to be proportional to $1/r$, which thus can capture far stars by releasing more latent heat in comparison to capturing near stars. Therefore, the gravitational force of the galaxy should be modified as

$$f = a \frac{GmM'}{r} + m \frac{GM}{r^2} = \begin{cases} m \frac{GM}{r^2} & \text{capturing 2D to 1D} \\ a \frac{GmM'}{r} & \text{capturing 3D to 1D} \end{cases} . \quad (38)$$

where the coefficient a only works in the far field of the gravity of the galaxy. In the viewpoint of the classical universal gravitational force, the far field attributes more unseen mass to the gravity effect, the unseen mass is recognized as the dark matter of the galaxy.

9. Sunspot formation

This section studies sunspot formation by comparing it with tropical cyclones on the earth.

These cyclones have established the following knowledge:

(1) tropical cyclone pregnancy basins are at a constructive interference ridge sandwiched between easterlies and westerlies, while zero wind in the ridge.

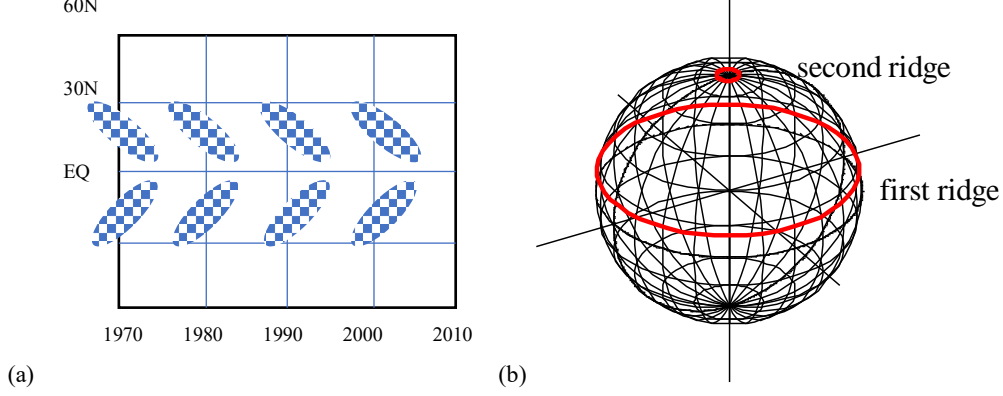


Fig.16 (a)Sunspot basins: latitudes vs. time. (b) In northern hemisphere, the first sun's constructive interference ridge swings between 0°N and 30°N, the second constructive interference ridge stays at the north pole.

```
<Clet2020 Script>// [26]
double beta,H,M,dp[20],D[2000],r,rs,rot,x,y,v1,v2,K1,K2,T1,T2,T,Lamda,V; int i,j,k,N;
int main(){beta=2.961520e10; H=SPEEDC*SPEEDC*SPEEDC/beta;
M=1.9891E30; rs=6.95e8;rot=2*PI/(25.05*24*3600);v1=rot*rs;K1=v1*v1/2//T1=2*PI*H/K1;
v2=0.7346*sqrt(BOLTZMANN*5700/MP)+0.2485*sqrt(BOLTZMANN*5700/(MP+MP));
K2=v2*v2/2;T2=2*PI*H/(K2-K1);T=T2/24*3600*365.2422;
Lamda=2*PI*H/(v2-v1);V=Lamda/T2;
SetViewAngle("temp0,theta60,phi-60");
DrawFrame(FRAME LINE,1,0xffaf);Overlook("2,1,60", D);
for(i=0;i<180;i+=15){k=0; K1=0; K2=i;Grid();}
for(i=0;i<180;i+=15){k=1; K1=i; K2=0;Grid();}
SetPen(3,0xff0000);k=1; K1=5; K2=0;Grid();K1=80; K2=0; Grid();
TextHang(10,30,60,"second ridge"); TextHang(50,50,10,"first ridge");
}
Grid();N=50; K1*=PI/180; K2*=PI/180; r=60;
if(k==0){v1=2*PI/N; v2=0;} else {v1=0; v2=2*PI/N;}
for(j=0;j<=N;j+=1){k=j+j;
D[k]=r*sin(K1)*cos(K2);D[k+1]=r*sin(K1)*sin(K2); D[k+2]=r*cos(K1);
K1+=v1;K2+=v2;} Plot("POLYGON,0,50, XYZ,10",D);
}#v07=?>A
```

The sunspot basins latitude vs. time as shown in Fig.16(a) tells us that sun's constructive interference ridge swings between 0°N and 30°N in the northern hemisphere, so do in the southern hemisphere. The first ridge's latitude angle A_1 in the northern hemisphere is written as

$$A_1 = A_0 [1 + \sin(\frac{2\pi t}{T_{sunspot}} + t_0)]; \quad A_0 = 15^\circ N; \quad T_{sunspot} = 11 \text{ years} . \quad (39)$$

with zero wind in the ridge. Zero wind also must hold at the two poles for the sake of geometric shape, therefore the north pole must accommodate the second ridge to stay, its latitude angle A_2 is supposed to be

$$A_2 \approx 90^\circ N - 0 \cdot \sin(\frac{2\pi t}{T_{pole}} + t_0); \quad T_{pole} = ? . \quad (40)$$

We immediately deduce that the second ridge's period T_{pole} equals to either $2T_{sunspot}$ or $0.5T_{sunspot}$, depending on the winds on the solar surface. The solar magnetic fields on the two poles flip every 22 years, which betrays a mystery: most probably to be $T_{pole} = 2T_{sunspot}$, regarding the second ridge as an undergoing-force to drive the solar magnetic fields on the two poles.

(2) Making use of the coherent width concept, and the spherical symmetry of shell's acceleration-roll wave.

Consider the interference between solar gas on the convective zone and the dense core's shell. The gas ψ_{gas} at the latitude angle A and the shell's ψ_{shell} at the same latitude are given by

$$\psi(r, A) = \psi_{gas}(r, A) + C\psi_{shell}(r, A) = \psi_{gas}(r, A) + C\psi_{shell_equator}(r)$$

$$T_{beat} \simeq \frac{4\pi c^3}{\beta(v_{gas}^2 - v_{shell_equator}^2)} \quad (41)$$

$$v_{shell_equator} = \omega r$$

$$v_{gas} = \omega r \cos(A) + v_{wind} + v_{convection_effect}$$

where C represents the coupling constant which relates to their distance and mass fractions within their coherent width, their interference leads to a beat phenomenon. The positive wind denotes the direction from west to east. The shell's ψ_{shell} takes at the equator due to the spherical symmetry of shell's acceleration-roll wave. We have known that there is a beat $T_{beat}=11$ years in the first constructive interference ridge with zero wind, using the above period formula we obtain the convective influence:

$$v_{v_{convection_effect}} = 6100 - \omega r \cos(A_1); \quad (units : m / s)$$

$$A_1 = A_0[1 + \sin(\frac{2\pi t}{T_{beat}} + t_0)]; \quad A_0 = 15^\circ N \quad (42)$$

In other words, the gas is subjected to the convective influence which enforces the beat oscillation in the ridge to run at the period $T_{beat}=11$ (years).

It is not easy to maintain the constructive interference condition for these waves. The wind required for maintaining the beat $T_{beat}=11$ (years) near the first ridge is calculated as shown in Fig.17(a) (blue line and red line), this wind will be destroyed by destructive interference at higher latitudes. But, the wind will arise up again at the second ridge where the waves satisfy the constructive interference condition: at $A=90^\circ N$ location where the beat $T_{beat_pole}=22$ (years).

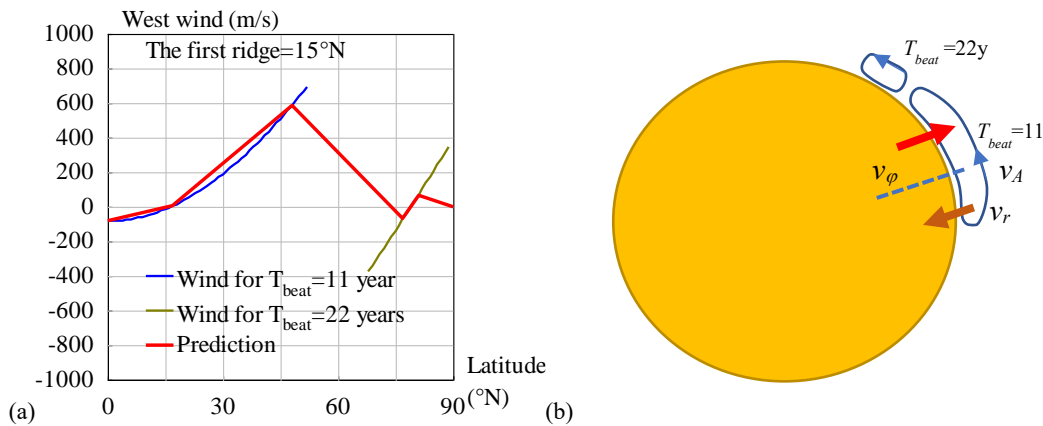


Fig.17 (a)Calculation of west winds required for the beat 11 years and 22 years in the northern hemisphere. (b)

The atmospheric circulation in the northern hemisphere.

```
<Clet2020 Script>// [26]
double beta,H,M,r,rc, rs,rot,v1,v2, Year,T,Lamda,V,a,b,w,N[500],F[100]; int i, j, k, t, m, n, f,Fmax,Type,x;
int main(){beta=2.961520e10; H=SPEEDC*SPEEDC*SPEEDC/beta;
M=1.9891E30; rs=6.95e8; rot=2*PI/(25.05*24*3600); Year=24*3600*365.2422; x=10;
SetAxis(X_AXIS,0,0,90,"Latitude#n(°N);0;30;60;90;");
SetAxis(Y_AXIS,-1000,-1000,1000,"West wind (m/s):-1000;-800;-600;-400;-200;0;200;400;600;800;1000;");
DrawFrame(0x016a,Type,0xaffaf);//Polyline(2,"-90,0,90,0");
```

```

Check(15,k); if(k>30) k=30; if(k<0) k=0;
T=22*Year; Wind(); f=0; Findf(); t=N[m+m]; T=11*Year; Wind(); f=0; Findf();
SetPen(2,0xff); Polyline(n,N,x,-400,"Wind for T#sdbeat#t=11 year");
F[0]=N[0]; F[1]=N[1]; F[2]=N[m+m]; F[3]=N[m+m+1]; t=(t+F[2])/2;//midpoint of two ridges
t=t-F[2]+m; Fmax=N[t+t+1]; //TextAt(100,20,"t=%d, Fmax=%f",t,Fmax);
f=Fmax; Findf(); F[4]=N[m+m]; F[5]=N[m+m+1];
T=22*Year; Wind(); f=-Fmax/10; Findf(); t=m; f=Fmax/10; Findf();
SetPen(2,0x80ff00); Polyline(n,N,x,-600,"Wind for T#sdbeat#t=22 years");
F[6]=N[t+t]; F[7]=N[t+t+1]; F[8]=N[m+m]; F[9]=N[m+m+1];
F[10]=90; F[11]=0;
SetPen(3,0xff0000); Polyline(6,F,x,-800,"Prediction");
TextHang(x,900,0,"The first ridge=%d°N", k);
}
Wind(){ n=0;
for(i=0;i<90;i+=1) { a=i*PI/180; v1=rot*rs*cos(a); v2=rot*rs; w=6100-v2*cos(k*PI/180);
a=4*PI*H/T+v2*v2; V=sqrt(a)-v1-w;
if(V>-400 && V<700) {N[n+n]=i; N[n+n+1]=V; n+=1;} }
Findf(){a=1e10; for(i=0;i<n;i+=1) { b=N[i+i+1]-f;if(b<0) b=-b;if(b<a) {m=i;a=b;} }
}
#v07=?>A

```

The maximal wind appears most probably at the midpoint of the two ridges, about 580m/s, linking all characteristic points in Fig.17(a) we obtain the predicted wind-curve over the northern hemisphere. The predicted second ridge has weak winds near the north pole, which agrees well with the judgment about the flipping of sun's geomagnetic field at the north pole.

For further improvement of precision, the value of the wind required by the constructive interference condition should be understood as a magnitude, it should be resolved into three components in the spherical coordinates (r, A, φ) as

$$v_{wind}^2 = v_r^2 + v_A^2 + v_\varphi^2 . \quad (43)$$

According to the energy equipartition theorem in thermodynamics, approximately we have the average estimation

$$\langle v_r^2 \rangle = \langle v_A^2 \rangle = \langle v_\varphi^2 \rangle = \frac{1}{3} v_{wind}^2 . \quad (44)$$

Thus, the wind vectors around the northern hemisphere of the sun are plotted in Fig.17(b), the atmospheric circulation consists of two cells: first cell, and second cell.

(3) Pregnancy mechanism of sunspots like tropic cyclones. The first constructive interference ridge sandwiched between easterlies and westerlies, where the shear action of the winds will produce a lot of vortexes if the winds are disturbed by the convective zone. The pregnancy of a sunspot needs three steps, as shown in Fig.18(a).

Step1, during active season, the stronger radiation output at higher altitudes over the warm surface and releases the $v_{convection_effect}$ into the gas at lower altitudes; consequently, the strengthened easterlies make a distortion to the first constructive interference ridge, as shown in Fig.18(a).

Step2, day by day, the distortion develops to an extent that it is going to separate from the mother-like first constructive interference ridge hit strongly by the westerlies, as shown in Fig.18(a).

Step3, finally, the distorted constructive interference ridge grows up to become an isolated baby ring which is recognized as a new sunspot, counter-clockwise in the northern hemisphere, as shown in Fig.18(a), similar to the famous large vortex on the surface of Jupiter.

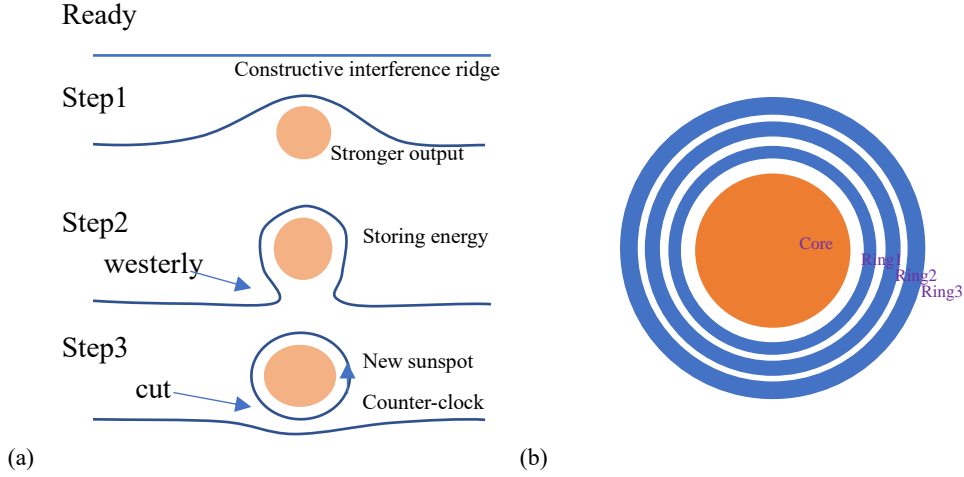


Fig.18 (a)Three steps of the pregnancy of a sunspot in the northern hemisphere. (b) Inner structure of a sunspot.

When the constructive interference ring of a newly born cyclone forms, its wavelength will adapt to the ring size as

$$\frac{1}{hM_{cyclone}} \oint_L v_l dl = 2\pi n; \quad n = 1, 2, \dots \quad (45)$$

$$\psi = \exp\left(\frac{i}{hM_{cyclone}} \int_0^x (u_1 dx_1 + u_2 dx_2 + u_3 dx_3 + u_4 dx_4)\right)$$

where the mass M represents the overall mass of the new cyclone, including the **imagined dark mass** which accounts for the latent heat released during its formation; the constant h is the **Planck-constant-like constant** determined by experimental observations. The air molecules of the ring are under the control of their acceleration-roll waves whose coherent length is so long that the waves have to overlap as

$$\psi(r) = 1 + e^{i\delta} + e^{i2\delta} + \dots + e^{i(N-1)\delta} = \frac{1 - \exp(iN\delta)}{1 - \exp(i\delta)} \quad (46)$$

$$\delta(r) = \frac{1}{hM_{cyclone}} \oint_L (v_l) dl$$

This formula can be used to calculate the distribution of the cyclone's nucleon density.

10. How 2D matter wave to obtain spin and how sunspot to spin

Dimension is defined as the number of independent parameters in a mathematical space. In the field of physics, dimension is defined as the number of independent space-time coordinates. 0D is an infinitesimal point with no length. 1D is an infinite line, only length. 2D is a plane, which is composed of length and width. 3D is 2D plus height component, has volume.

In this section we at first discuss how to measure dimension by wave. In Fig.19(a), one puts earphone into ear, one gets 1D wave in the ear tunnel.

$$1D: \quad y = A \sin(kr - \omega t) = \frac{A}{r^0} \sin(kr - \omega t) \quad (47)$$

where r is the distance between the wave emitter and the receiver. In Fig.19(b), one touches a guitar spring, one gets 2D cylinder wave.

$$2D: y = \frac{A}{r^{1/2}} \sin(kr - \omega t). \quad (48)$$

In Fig.19(c), one turns on a music speaker, one gets 3D spherical wave.

$$3D: y = \frac{A}{r} \sin(kr - \omega t). \quad (49)$$

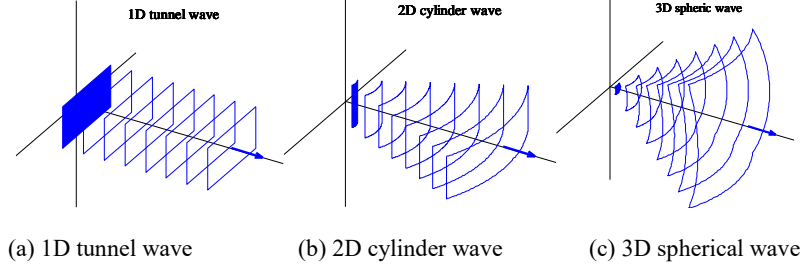


Fig.19 The wave behavior in various dimensional spaces.

```
<Clet2020 Script>// Clet is a C compiler [26]
int i,j,k,type,nP[10]; double D[20],S[1000];
int main(){SetViewAngle("temp0,theta60,phi-30");SetAxis(X_AXIS,0,0,200,"X;0;200;");
DrawFrame(FRAME_LINE,1,0xafffaf); type=2;SetPen(1,0x00ff);
for(i=10;i<160;i+=20){D[0]=i;D[1]=0;D[2]=0;D[3]=i+5;D[4]=0;D[5]=0;D[6]=i;D[7]=10;D[8]=0;
if(type==0) {D[9]=4;D[10]=40;D[11]=20;D[12]=i;TextHang(50,0,100,"1D tunnel wave");k=CARD;}
else if(type==1) {D[9]=200;D[10]=i/2;D[11]=20;D[12]=i;TextHang(50,0,100,"2D cylinder wave");k=50;}
else {D[9]=200;D[10]=i/2;D[11]=i/2;D[12]=i;TextHang(50,0,100,"3D spheric wave");k=40;}
Lattice(k,D,S);nP[0]=POLYGON;nP[1]=0;nP[2]=200;nP[3]=XYZ;
if(i==10) nP[1]=3; if(type==0) nP[2]=4; Plot(nP,S[9]);}
j=30;D[3]=D[0]+j*S[0];D[4]=D[1]+j*S[1];D[5]=D[2]+j*S[2];
SetPen(3,0x00ff);Draw("ARROW,0,2,XYZ,10",D);}
#v07=?>A
```

In general, we can write a wave in the form

$$y = \frac{A}{r^w} \sin(kr - \omega t). \quad (50)$$

It is easy to get the dimension of the space in where the wave lives, the dimension is $D=2w+1$. Nevertheless, wave can be used to measure the dimension of space, just by determining the parameter w .

Waves all contain a core oscillation ([vibration invariance](#). Hubble's law not only tells us about redshift, but also clarifies the real situation in a sense: vibration invariance.)

$$\frac{d^2 y}{dr^2} + k^2 y = 0, \quad (51)$$

Substituting y into the core oscillation, we obtain the radial wave equation

$$\frac{d^2 y}{dr^2} + \frac{2w}{r} \frac{dy}{dr} + (k^2 + \frac{w(w-1)}{r^2}) y = 0. \quad (52)$$

This equation expresses the wave behavior modulated by the spatial dimension parameter w . For 1D wave $w=0$, it is trivial, but for 2D wave $w=1/2$, it reduces to the Bessel equation in a cylinder coordinate system (r, φ)

$$\frac{d^2 y}{dr^2} + \frac{1}{r} \frac{dy}{dr} + \left(k^2 - \frac{1}{4r^2}\right)y = 0 \quad (2D \text{ wave})$$

comparing to the Schrodinger's equation: (53)

$$\frac{d^2 R(r)}{dr^2} + \frac{2}{r} \frac{dR(r)}{dr} + \left[k^2 - \frac{l(l+1)}{r^2}\right]R(r) = 0$$

In quantum mechanics, y is an electronic wave function, comparing to the Schrodinger radial wave equation in textbooks, we find that the $-1/4r^2$ term represents the electronic spin effect. However, here according to the above radial Bessel equation we can simply conclude that sound wave, electromagnetic wave, or any wave can have spin effect in 2D space! Let us use k denote the wave-vector, then the above 2D wave equation tells us

$$k_r^2 = k^2 - k_\phi^2; \quad k = \frac{2\pi}{\lambda}; \quad k_\phi = \pm \frac{1}{2r}. \quad (54)$$

The k_ϕ causes the 2D wave-vector k to spin little by little as illustrated Fig.20. The positive and negative k_ϕ corresponds to spin up and spin down respectively; as r goes to the infinity, the spin effect vanishes off.

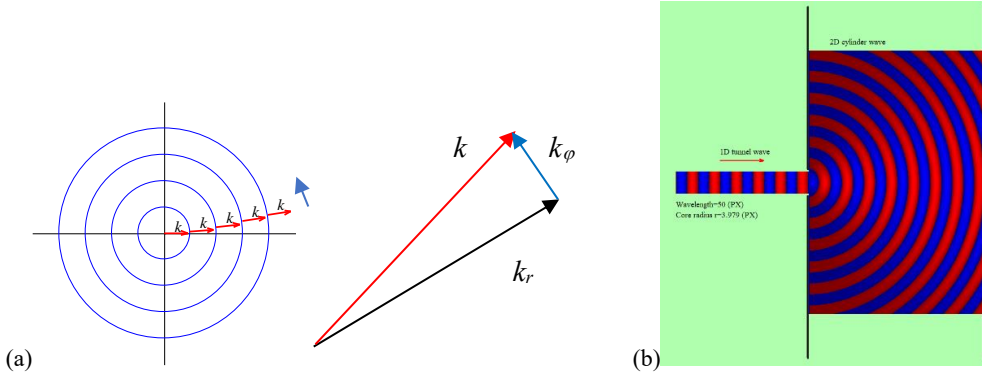


Fig.20 (a) 2D wave-vector k spins little by little in the cylinder coordinates (r, ϕ) . (b) from 1D to 2D, the spin works to split the electron beam due to double-value k_ϕ .

```
<Clet2020 Script>// Clet is a C compiler [26]
int i,j,k;double r,x,y,a,D[100];
int main(){DrawFrame(FRAME_LINE,1,0xffffaf); SetPen(1,0x0000ff);
for(i=0;i<90;i+=20){D[0]=-i;D[1]=-i;D[2]=i;D[3]=i; Draw("ELLIPSE,0,2,XY,0",D);}
for(i=0;i<90;i+=20){a=0.2*(i-i*200)*PI/180;r=i;D[0]=r*cos(a);D[1]=r*sin(a);
r+=18;D[2]=r*cos(a);D[3]=r*sin(a); SetPen(2,0xffff00);
Draw("ARROW,0,2,XY,8",D);TextHang(D[2]-10,D[3]+5,0,"#ifk");}
}#v07=?>A
```

If the 2D wave is the de Broglie matter wave for a particle beam, in a cylinder coordinate (r, ϕ) , then the matter wave has a spin angular momentum given by

$$k_r = \frac{p_r}{\hbar}; \quad k_\phi = \frac{p_\phi}{\hbar} = \frac{J_\phi}{r\hbar}; \quad J_\phi = \pm \frac{1}{2}\hbar. \quad (55)$$

According to the angular momentum formula in general physics, it is recognized that the particle total momentum p is a constant given by

$$\left(\frac{p}{\hbar}\right)^2 = \left(\frac{p_r}{\hbar}\right)^2 + \left(\frac{p_\phi}{\hbar}\right)^2. \quad (56)$$

$$k^2 = k_r^2 + k_\phi^2 = \text{const.}$$

Since the particle total wave vector k is a constant, the wave-vector k_r must vary as r changes.

The wave-vector in the radial direction would change as the wave attenuates.

Most physicists obtain redshift information from the Hubble law, but few physicists may think that the Hubble law implies invariance of wavelength on the solar-size scale, called as the vibration invariance. Consider a 2D matter wave emitting from a source with the wave vector $k=2\pi/\lambda$, there is a critical radius r_u where

$$k_r |_{r=r_u} = 0; \quad k_\phi = \frac{1}{2r_u} = k = \frac{2\pi}{\lambda}; \quad (57)$$

Within the area $r < r_u$, we deduce that $k_r=0$; while the outside area $r > r_u$, we deduce that k_r gradually grows as r grows until its spin component vanishes, crossing the boundary $r=r_u$ gives rise an uncertainty: left-hand spin or right-hand spin. Thus, the critical radius r_u is called as uncertainty radius, the area within $r < r_u$ is called uncertainty core.

Due to some mechanism, suppose the left-hand spin retains, as illustrated in Fig.21(a). At the first, it is found that the wave progression in r direction within the uncertainty core is banned, that is $k_r=0$ because of $k_\phi=k$, showing a quantum vortex structure; Next, if few matters leaking from the core spread out, they will bring away an amount of angular momentum from the source. For a stationary source, the leakage of angular momentum must be banned, on the boundary of the uncertainty radius, a convective array would form with which the wave progression erupts out from the gap of the convective array, in this case the convective array recycles almost all angular momentum leaked, as illustrated in Fig.21(b). The third, the circular component k_ϕ within the uncertainty core must be in a superfluid state, otherwise it will die in a shorter time due to dissipative motion, the uncertainty core must be a quantum superfluid vortex.

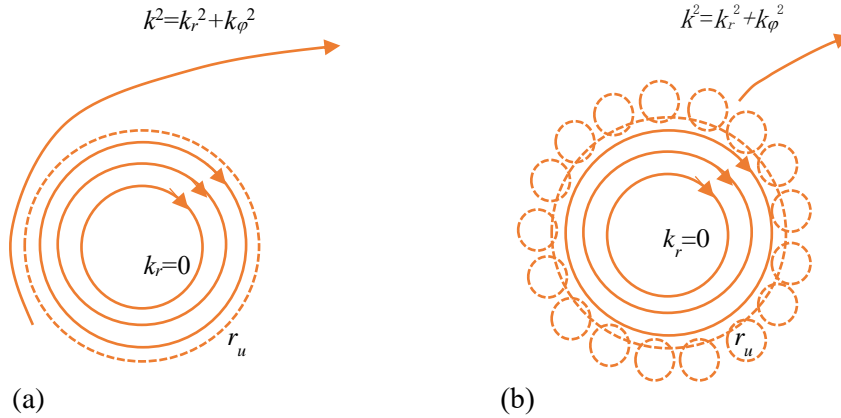


Fig.21 (a) The wave progression brings away an amount of angular momentum from the source, must be banned.
(b) The convective array recycles almost all angular momentum leaked.

Now come back to astrophysics where acceleration-roll waves govern all quantum gravity effects. For resisting the leakage of angular momentum due to the emission or absorption of acceleration roll waves on the solar system 2D plane, both the Sun and Earth have self-rotation and have convective zone in atmosphere, as shown in Fig.21(b).

In the preceding section, we have mentioned there are two constructive interference ridges

on the solar northern hemisphere, the first ridge locates at the latitude $A=15^\circ\text{N}$ where the beat $T_{beat}=11$ (years), the second ridge is near the north pole where the latitude about $A=90^\circ\text{N}$ where the beat $T_{beat_pole}=22$ (years), as shown in Fig.22(a). When the acceleration-roll wave varies at the first ridge, correspondently, the $|\psi|^2$ density variation produces a series of sunspots around the first ridge. Each sunspot acts as a quantum superfluid vortex as shown in Fig.22(b), the circular vortex would push the lighter electrons to move faster than the massive ions, thus the superfluid electrons yield a magnetic field whose direction is in the solar radius direction or the solar radiation direction, as shown in Fig.22(b), the magnitude of sunspot's magnetic field is about 0.1—0.5 Tesla according to experiment measurements. When the acceleration-roll wave varies at the second ridge, the $|\psi|^2$ density variation produces several sunspots around the north pole, each acts as a quantum superfluid vortex as shown in Fig.22(b), the circular vortex would push the lighter electrons to move faster than the massive ion, thus the superfluid electrons yield a magnetic field whose direction is in the north pole direction, the magnitude of magnetic field is less than 0.1 Tesla according to experiment measurements, the size of the sunspots at the north pole would be bigger than that at the first ridge. The sunspots near the north pole and south pole with a beat $T_{beat_pole}=22$ (years) construct up the solar alternating geomagnetic field. According to the preceding section, cyclones in two poles control the orientation of the solar geomagnetic field, and the cyclone's orientation flips every 22 years.

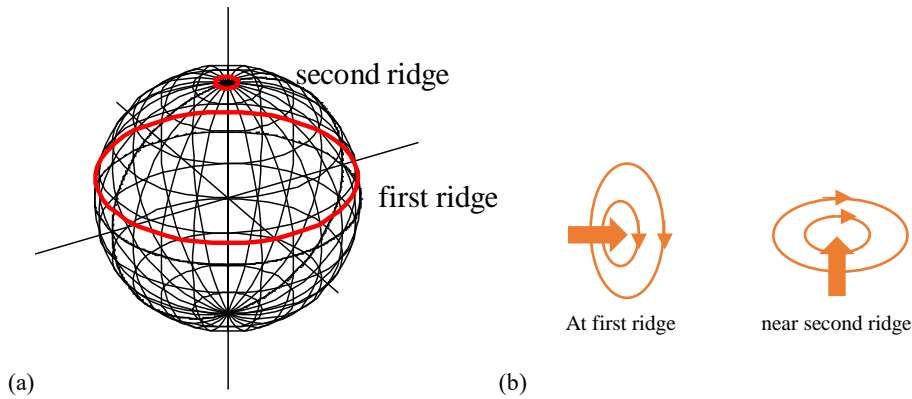


Fig.22 (a) There are two constructive interference ridges on the solar northern hemisphere. (b) The sunspots near the equator and north pole.

Why the electron flow in sunspot is superfluid? Imagining an electron flow which collides with a positive ion flow, transfers an amount of energy ΔE to the ion flow. But, because the matter flow within uncertainty core in circular motion without radial flow, theoretically $k_r=0$, it cannot transport the energy ΔE into its surroundings so that it has to deliver back the energy ΔE to the electron flow, as consequence, the electron flow runs circular motion without energy lose or energy gain during the collision with the ion flow, therefore, the electron flow in sunspot is superfluid.

How the circular vortex to push the lighter electrons to move faster than the massive ions? The most probable speed of gas is the speed of at which the probability is maximum, that is

$$v_p = \sqrt{\frac{2RT}{M}}. \quad (58)$$

During the formation of the circular vortex within the uncertainty core, the gas has to experience

a dimension change from 2D to 1D motion, the gas has to redistribute its kinetic energy to support the electron flow and ion flow, the motion in r direction must vanish as follows

$$2D \begin{cases} E_\theta = \frac{1}{2} M v_\varphi^2 \Rightarrow E_{\varphi_thermal} \\ E_r = \frac{1}{2} M v_r^2 \Rightarrow E_{\varphi_flow} \end{cases} . \quad (59)$$

The thermal kinetic energy in the φ direction retains; while thermal kinetic energy in the r direction transforms into the circular flow energy (suppose the left-hand spin retains). Therefore, the formula of most probable speed of gas can be used to estimate the speed v_{e_flow} of electron flow and the speed v_{ion_flow} of ion flow, they are

$$\frac{v_{p-e}}{v_{p-ion}} = \sqrt{\frac{M_{ion}}{M_e}}; \Rightarrow \frac{v_{e_flow}}{v_{ion_flow}} = \sqrt{\frac{M_{ion}}{M_e}} . \quad (60)$$

Where M_e is the mass of electron, M_{ion} is the mass of proton.

Why the center of sunspot has a lower temperature? The sunspot acts as a quantum superfluid vortex, finally maintaining the same angular speed ω so that the center flow has a lower speed and at a lower temperature.

11. Geomagnetic field

The earth is in a stationary state, in the earth's core there are molten iron flows in circular motion, regarding it as the residue vortex on the equatorial 2D plane after a long-term cooling process. The circular vortex iron flow would push the lighter electrons to move faster than the massive ions, thus the superfluid electrons yield a magnetic field whose direction is in the south pole direction. The circular vortex electron flows construct up the earth's geomagnetic field.

The earth's geomagnetic field is difficult to change its orientation, because the earth's atmosphere is non-conductive, the earth's magnetic field is mainly generated by the electron-flows in the earth's molten matters. Although some geologists speculate the existence of earth's magnetic reversals, however there has not been a reversal in nearly 800 kiloyears. In earth's history, reversals are possible only when its matter waves were assaulted and destroyed by internal high temperatures or external strong plasma winds from exotic events. Measurements indicate that earth's magnetic field has weakened by about 10% since 1800s.

Now let us calculate the earth's magnetic field B at the north pole. The earth radius is $r_s=6378\text{km}$ with angular speed $\omega=2\pi/(24*3600)$; the radius of molten core takes $R= r_s/2$. The molten core consists of electron flows and Fe ion flows. The speed of circular electron flow, as shown in Fig.23, is given by

$$v_{e_flow} = v_{ion_flow} \sqrt{\frac{56M_{proton}}{M_e}} = \omega R \sqrt{\frac{56M_{proton}}{M_e}} . \quad (61)$$

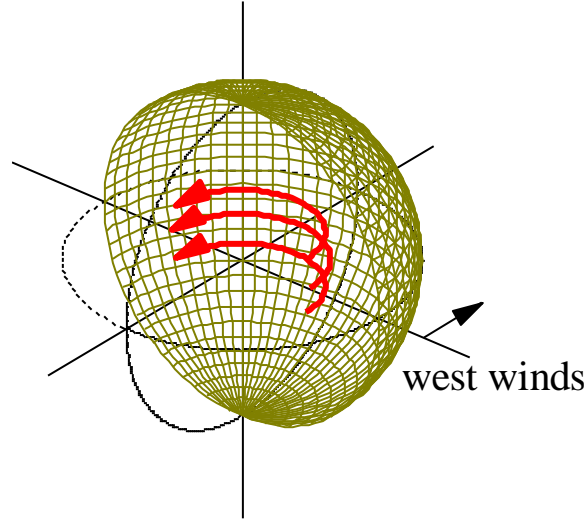


Fig.23 West winds in the interior of sun or earth, easterlies are negative west winds.

```
<Clet2020 Script> [26]
double dP[20],D[2000],r,v1,v2,K1,K2; int i,j,k,N;
int main(){ N=50; r=60; dP[0]=POLYLINE;dP[1]=0;dP[2]=N+1;dP[3]=XYZ;dP[4]=16;
SetViewAngle("temp0,theta60,phi-40");
DrawFrame(FRAME LINE,1,0xafffaf);Overlook("2,1,60", D);
Draw("ARROW,0.2,XYZ,16","80,0,0,80,30,0"); TextHang(70,0,-20,"west winds");
SetPen(1,0xed9121); for(i=0;i<=180;i+=5) {k=0; K1=0; K2=i; Grid();}
for(i=0;i<=180;i+=5) {k=1; K1=i; K2=0; Grid();}
//TextAt(10,10,"v1=%d, v2=%d, T=%.2f y, λ=%e, V=%d",v1,v2,T, Lamda,V);
SetPen(3,0xff0000); k=1; K1=70; K2=0;r=30; dP[1]=3; Grid();
K1=90; K2=0;r=30; dP[1]=3; Grid(); K1=110; K2=0;r=30; dP[1]=3; Grid();
}
Grid(); K1*=PI/180; K2*=PI/180;
if(k==0) {v1=PI/N; v2=0;} else {v1=0; v2=PI/N;}
for(j=0;j<=N;j+=1){ k=j+j+j;
D[k]=r*sin(K1)*cos(K2);D[k+1]=r*sin(K1)*sin(K2); D[k+2]=r*cos(K1);
K1+=v1;K2+=v2; }Plot(dP,D);
}#v07=?>A#t
```

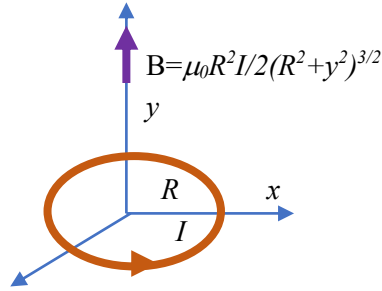


Fig.24 The magnetic field of a single coil.

The n_e denotes the conducting electron density, according to the magnetic field formula of a single coil, as shown in Fig.24, the B is given by

$$B = \int_{r=0}^{r=r_s/2} \int_{A=-\pi/2}^{A=\pi/2} \frac{\mu_0 R^2 n_e v_e r dr dA}{2(R^2 + (r_s - r \sin A)^2)^{3/2}}; \quad R = r \cos A \quad (62)$$

$$n_e = 8e + 10(m^{-3}); \quad B = 0.62(Gauss)$$

```
<Clet2020 Script> [26]
double beta,H,M,r,rc,rs,rot,ne,V,R,A,B,D,a,b,d,m,v1,v2,T,Year; int i,j,k;
int main(){ Year=24*3600*365.2422;
```

```

beta=2.961520e10; H=SPEEDC*SPEEDC*SPEEDC/beta;
M=1.9891E30; beta=1.377075e+14; H=SPEEDC*SPEEDC*SPEEDC/beta;
M=5.97237e24; rs=6.378e6; rot=2*PI/(24*3600);D=56*MP/ME;D=sqrt(D);
B=0; a=rs/200; b=PI/100; ne=8e10;
for(i=1;i<100;i+=1) { r=a*i; for(j=0;j<100;j+=1) { A=b*(j-50); R=r*cos(A); V=rot*R*D;
d=rs-r*sin(A); d=R*R+d*d; d=sqrt(d); d=2*d*d*d;
B+=MC*R*R*CHARGE*ne*V*r/d; }}
B=B*a*b; m=ne/AVOGADRO;
TextAt(100,100,"ne=%e, m=%e, B=%e", ne, m, B);
v1=rot*rs/2; v2=0; T=4*PI*H/(v1*v1-v2*v2);T=T/Year;
TextAt(100,200,"v1=%e, v2=%e, T=%f y",v1,v2,T);
}#v07=?>A

```

By fitting data, if the conducting electron density takes $n_e = 8e+10(m^{-3})$, then we obtain the earth's geomagnetic field at the north pole $B=0.62$ Gauss, which is consistent with experimental observation. To note that the conducting electron density is very thin, about $1.3e-13(/mole)$. Mars and Venus are either too small to have a convective core or rotate very slowly, so they are with weak or no magnetic fields.

12. Insight into electronic spin in atoms

As shown in Fig.25(a), if the coherent length of the electron in a hydrogen atom is long enough, it will wind around the time axis, the matter wave in the circle will overlap, and interfere with itself at every location. The overlapping number N depends on the coherent length L ; if $N=\infty$, the matter wave has the interference like the Fabry-Perot interference in optics.

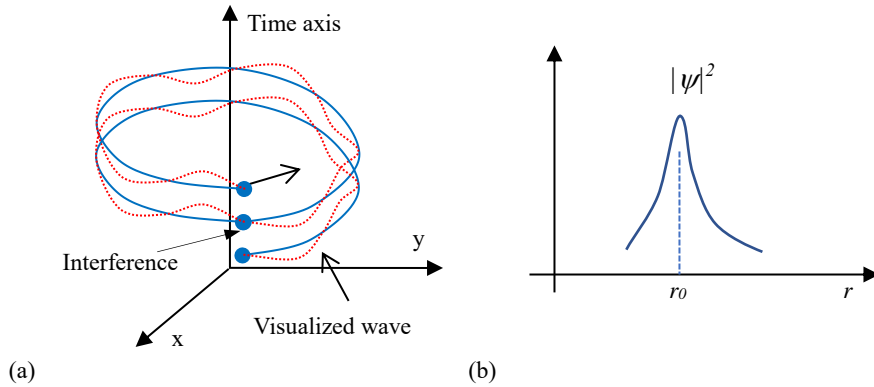


Fig.25 (a)The matter wave winds around the time axis, overlap and interfere with itself. (b)The distribution of overlapped 2D matter wave about its Bohr' radius.

The overlapped matter wave is given by

$$\psi = w + we^{i\delta} + we^{i2\delta} + \dots we^{i(N-1)\delta} = w \frac{1 - \exp(iN\delta)}{1 - \exp(i\delta)} \quad (63)$$

$$\delta = \frac{1}{\hbar} \oint_L p dl$$

where, δ is the phase shift after one circle retardation for the matter wave. Obviously, the Bohr orbits can survive only if the denominator of the above equation is satisfied by

$$\delta = \frac{1}{\hbar} \oint_L p dl = 2\pi n; \quad n = 1, 2, 3, \dots \quad (64)$$

For a 2D Bohr orbit, in the φ direction and in the r direction, the 2D wave function expresses

as $\psi = \Phi(\varphi)R(r)$. The self-interference of the winding matter wave would enhance its attenuation about the Bohr radius r_0 in the radial direction, shown in Fig.25(b). For the slope-up side and the slope-down side about the r_0 , as shown in Fig.26, it easily estimates the wave function in a composite state as follows

$$\begin{aligned} r \leq r_0 : R(r,t) &\approx \left(\frac{r_0}{r}\right)^{-j_1} \left(\frac{r_u}{r}\right)^{1/2} \sin(kr - \omega t) \\ r > r_0 : R(r,t) &\approx \left(\frac{r_0}{r}\right)^{j_2} \left(\frac{r_u}{r}\right)^{1/2} \sin(kr - \omega t) \end{aligned} \quad (65)$$

where the parameter j determines the slope of the attenuation in the r direction, **the half number 1/2 is prepared for the spin concept.**

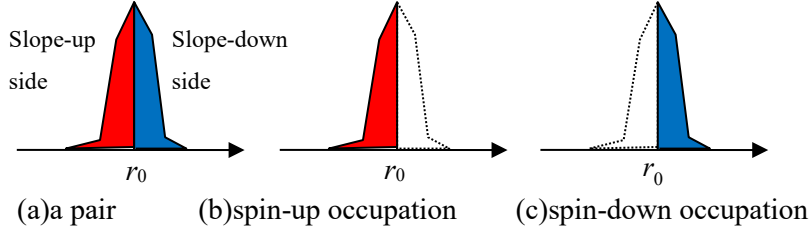


Fig.26 The orbit accommodates one spin-up and another spin-down electrons.

To note that the sinusoidal function in the above expressions is the invariant core of this oscillation

$$\left(\frac{d^2}{dr^2} + k^2\right)R = 0 \quad (66)$$

which holds **vibration invariance** by keeping $k = \text{constant}$. Substituting R into it, these wave functions actually have to satisfy the Bessel-like equations:

$$\begin{aligned} r \leq r_0 : w &= -j_1 + \frac{1}{2}, \\ \frac{d^2 R}{dr^2} + \frac{2(-j_1 + \frac{1}{2})}{r} \frac{dR}{dr} + [k^2 + \frac{(j_1 + \frac{1}{2})(j_1 - \frac{1}{2})}{r^2}]R &= 0 \end{aligned} \quad (67)$$

$$\begin{aligned} r > r_0 : w &= j_2 + \frac{1}{2}, \\ \frac{d^2 R}{dr^2} + \frac{2(j_2 + \frac{1}{2})}{r} \frac{dR}{dr} + [k^2 + \frac{(j_2 + \frac{1}{2})(j_2 - \frac{1}{2})}{r^2}]R &= 0 \end{aligned}$$

Because the total wave vector k^2 is a constant, these equations become the equations governing the wave behavior. Their solutions are approximately given by

$r \leq r_0$:

$$R(r, t) = \left(\frac{r_0}{r}\right)^{-j_1} \left(\frac{r_u}{r}\right)^{-1/2} \sin\left(r\sqrt{k_r^2 - \frac{(j_1 + \frac{1}{2})(j_1 - \frac{1}{2})}{r^2}} - \omega t + \phi\right) + O\left(\frac{1}{r^{3+j_1}}\right)$$

$r > r_0$:

$$R(r, t) = \left(\frac{r_0}{r}\right)^{j_2} \left(\frac{r_u}{r}\right)^{1/2} \sin\left(r\sqrt{k_r^2 - \frac{(j_2 + \frac{1}{2})(j_2 - \frac{1}{2})}{r^2}} - \omega t\right) + O\left(\frac{1}{r^{3+j_2}}\right)$$

(68)

The slope-up range accommodates the spin-up electron; the slope-down range accommodates the spin-down electron; thus, one orbit accommodates a pair of electrons.

Comparing to the Schrödinger wave equation, it is easy to find that j takes place at the site "orbital angular momentum quantum number". In a spherical 3D coordinate $(r; \theta, \varphi)$, we find that j was called as the quantum number in the θ direction. Indeed, here the attenuating parameter j would automatically be quantized in this quantum system as it plays the role of angular momentum in the above equations.

We argue that there is not motion in the θ direction in our 2D planet model in the cylinder coordinates $(r; \varphi)$; the j is just an attenuating parameter of the composite matter wave about its Bohr radius r_0 , depending on the overlapping number N . So that the attenuating parameter j is a **disguised freedom**, because of this disguised freedom, the electron motion in atoms was mistakenly explained as 3D motion for a hundred years.

Experimental evidence shows: magnetic needles would flip in a magnetic field; the atomic magnetic moment corresponding to the motion in the θ direction in the 3D mode cannot be flipped in external magnetic field, this experimental observation indicates that the atomic angular momentum in the θ direction in 3D model does not exist; only the attenuating parameter j enable to allow **the magnetic moment no-flipping in external field, because the j represents a disguised freedom**.

Electrons in atoms move in a 2D motion like in planetary orbits, but for a hundred years the electron motion in atoms was mistakenly explained as 3D motion in modern physics, actually this big mistake had made serious harm to the modern physics.

How to calculate atomic magnetic moment? If the orbit accommodates a pair of electrons, the two electrons must chase each other in the φ direction, because heading to each other would collide with each other frequently and exhaustedly. The total angular momentum should take both contributions into account as follows

$$\begin{aligned} J_\varphi &= \sqrt{(j_1 + \frac{1}{2})(j_1 - \frac{1}{2})}\hbar \pm \sqrt{(j_2 + \frac{1}{2})(j_2 - \frac{1}{2})}\hbar \\ &= m\hbar; \quad m = 0, \pm 1, \dots \end{aligned} \quad (69)$$

Experiments tell us there is not magnetic moment for the pair of electrons, that is

$$J_\varphi = 0; \quad j_1 = j_2; \quad m = 0; \quad (70)$$

Although the total angular momentum and total magnetic moment are zero, the electrons both still have their chasing motion in the φ direction (if parameter $j_2+1/2$ is defined as the positive

direction, then parameter $-j_1+1/2$ is defined as the negative direction), i.e. their combined spin angular momentum is invisible for external magnetic field.

If the orbit accommodates a single spin-down electron, its angular momentum is

$$J_\varphi = \sqrt{(j_2 + \frac{1}{2})(j_2 - \frac{1}{2})}\hbar = m\hbar \quad (71)$$

where, the electron must subject to the orbital quantization conditions

$$\begin{aligned} \frac{2}{\hbar} \int_{r_{\min}}^{r_{\max}} p_r dx &= 2\pi n_r, \quad n_r = 0, 1, 2, \dots \\ \frac{1}{\hbar} \int_0^{2\pi} p_\varphi r d\varphi &= 2\pi m, \quad m = \pm 1, \pm 2, \dots \end{aligned} \quad (72)$$

The single electron spin is towed up by the dimension parameter j_2 . The atomic magnetic moment is given by

$$\mu = \frac{e}{2m_e} J_{total} = \frac{e}{2m_e} J_\varphi = \frac{e}{2m_e} m\hbar \quad (73)$$

$$J_{total} = J_\varphi = m\hbar = [(m - \frac{1}{2})\hbar + \frac{1}{2}\hbar] = [(m - \frac{1}{2})\hbar + |J_{spin}|] \quad (74)$$

The spin angular momentum is enveloped by the total angular momentum.

13. Stern-Gerlach experiment and Lander factor

In general, it is hard in macroscopic scale to separate the left-turn electrons and right-turn electrons in a 2D matter wave, except under certain conditions in some deliberately designed magnetic apparatus. In Stern-Gerlach experiments, as shown in Fig.27(a), silver (Ag) atoms are heated in an oven, the oven has a small hole through which some silver atoms escape. The silver vapor busts out the oven and go through a slit as the collimator and is then subjected to an inhomogeneous magnetic field. In this experiment, the single valent election of silver atom moves in its Bohr orbit, as shown in Fig.27(b), we adopt a cylinder coordinates (r, φ) with the origin at the sliver center.

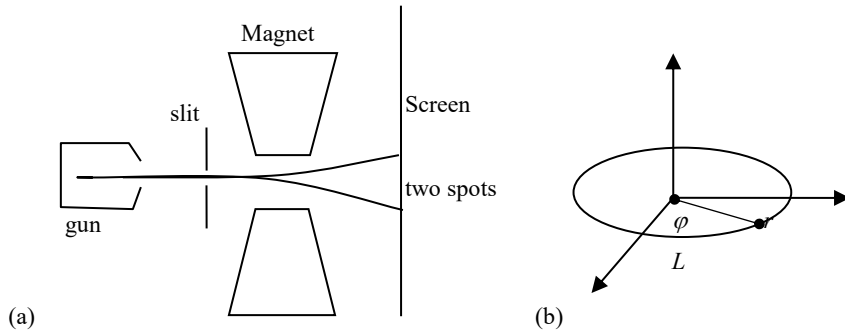


Fig.27 The Stern-Gerlach experiment apparatus.

As shown in Fig.28(a), if the coherent length of the electron in a hydrogen atom is long enough, it will wind around the time axis, the matter wave in the circle will overlap, and interfere with itself at every location. The overlapping number N depends on the coherent length L ; if $N=\infty$,

the matter wave has the interference like the Fabry-Perot interference in optics.

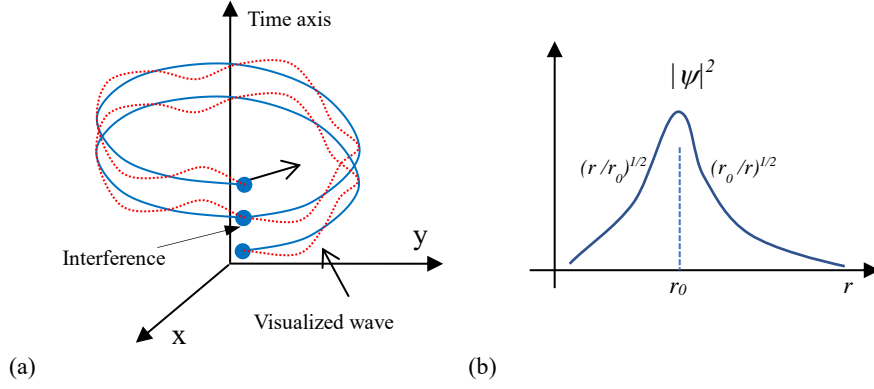


Fig.28 (a)The matter wave winds around the time axis, overlap and interfere with itself. (b)The distribution of overlapped 2D matter wave about its Bohr' radius.

The overlapped matter wave is given by

$$\psi = w + we^{i\delta} + we^{i2\delta} + \dots we^{i(N-1)\delta} = w \frac{1 - \exp(iN\delta)}{1 - \exp(i\delta)} \quad (75)$$

$$\delta = \frac{1}{\hbar} \oint_L p dl$$

where, δ is the phase shift after one circle retardation for the matter wave. Obviously, the Bohr orbits can survive only if the denominator of the above equation is satisfied by

$$\delta = 2\pi n; \quad n = 1, 2, 3, \dots \quad (76)$$

For a 2D Bohr orbit, in the φ direction and in the r direction, the 2D wave function is written as $\psi = \Phi(\varphi)R(r)$, consider a simplest case as shown in Fig.28(b), the overlapped matter wave of a silver atom with a finite N is approximately given by

$$\Phi(\varphi) = \exp\left(\frac{ip_\varphi}{\hbar} r\varphi\right); \quad R(r) = \begin{cases} \sqrt{\frac{r_0}{r}} \exp\left(\frac{ip_r}{\hbar} r\right) = \sqrt{\frac{r_0}{r}} & p_r = 0 \quad r > r_0 \\ \sqrt{\frac{r}{r_0}} \exp\left(\frac{ip_r}{\hbar} r\right) = \sqrt{\frac{r}{r_0}} & p_r = 0 \quad r < r_0 \end{cases} \quad (77)$$

Although $p_r=0$, the fact was omitted by almost all of us, the wave function in a 2D cylinder wave ($r > r_0$) satisfies

$$\frac{d^2 R}{dr^2} + \frac{1}{r} \frac{dR}{dr} + \left[k^2 + \frac{1}{2} \left(\frac{1}{r} - 1 \right) \right] R = 0 \quad (78)$$

Because the single valent election of silver atom lives in a 2D orbital space, acquiring the extra spin angular momentum, the Ag atom has a magnetic moment

$$J_{spin} = \pm \frac{1}{2} \hbar \Rightarrow \mu = g \frac{e}{2m} J_{spin} \quad (79)$$

where g is the Lander factor, $g=2$. Because the interaction energy of the magnetic moment with the magnetic field is just $-\mu B$, the z -component of the force experienced by the silver atom is

given by

$$f_z = \frac{\partial}{\partial z}(\mu B) = \mu \frac{\partial B}{\partial z}. \quad (80)$$

where we have ignored the components of B in direction other than the z - direction. In the z direction, the silver atom beams, 50% atoms experience an upward force, and other 50% atoms experience a downward force, thus on the screen we get the view there are two spots, in agreement with the theoretical prediction.

Why did physics introduce the Lander factor? In fact, there are two kinds of angular momentum we should consider in the φ direction

$$\begin{aligned} J_{total} &= J_{\varphi} = \pm \hbar \\ J_{spin} &= \pm \frac{1}{2} \hbar \end{aligned} \quad (81)$$

The spin needs to occupy the half of the total angular momentum in this case, in other words the total angular momentum contains the spin angular momentum, that is

$$J_{total} = J_{\varphi} = \pm \left(\frac{1}{2} \hbar + \frac{1}{2} \hbar \right) = \pm \left(\frac{1}{2} \hbar + |J_{spin}| \right). \quad (82)$$

In other words, the spin angular momentum is enveloped by the total angular momentum. Thus, we obtain the normal magnetic moment which should be

$$\begin{aligned} \mu &= \frac{e}{2m} J_{total} = \frac{e}{2m} J_{\varphi} = \frac{e}{2m} 2J_{spin} = \frac{e}{2m} g J_{spin}. \\ \therefore g &= 2 \end{aligned} \quad (83)$$

The external magnetic field can only probe the total magnetic moment, but fails to directly detect the enveloped-inside spin angular momentum, we need the Lander factor to grip on the spin concept.

14. Conclusions

In analogy with the ultimate speed c , there is an ultimate acceleration β , nobody's acceleration can exceed this limit β , in the solar system, $\beta=2.961520e+10(m/s^2)$. Because this ultimate acceleration is large, any effect related to β will become easy to test, including quantum gravity tests. In this paper, an approach is put forward to connect the ultimate acceleration with quantum theory, and is applied to sunspot, earth's tropic cyclones, and earth's geomagnetic field problems. The sunspot cycle is calculated to be 10.93 years due to the ultimate acceleration. A simulation was carried out, clearly showing the inner structure of a cyclone, which is consistent with the famous DIANA cyclone on 12 September 1984 in situ observation measured by an aircraft. The sunspot structure is also investigated, which has a similarity to that of a tropic cyclone. The ultimate acceleration provides a mechanism to explain geomagnetic field, the earth's geomagnetic field is calculated to be 0.6Gauss at the north pole.

References

- [1]C. Marletto, and V. Vedral, Gravitationally Induced Entanglement between Two Massive Particles is Sufficient Evidence of Quantum Effects in Gravity, Phys. Rev. Lett., 119, 240402 (2017)
- [2]T. Guerreiro, Quantum effects in gravity waves, Classical and Quantum Gravity, 37 (2020) 155001 (13pp).

- [3]S. Carlip, D. Chiou, W. Ni, R. Woodard, Quantum Gravity: A Brief History of Ideas and Some Prospects, *International Journal of Modern Physics D*, V,24,14,2015,1530028. DOI:10.1142/S0218271815300281.
- [4]de Broglie, L., *CRAS*,175(1922):811-813, translated in 2012 by H. C. Shen in *Selected works of de Broglie*.
- [5]de Broglie, Waves and quanta, *Nature*, 112, 2815(1923): 540.
- [6]de Broglie, Recherches sur la théorie des Quanta, translated in 2004 by A. F. Kracklauer as *De Broglie, Louis, On the Theory of Quanta*. 1925.
- [7]NASA, <https://solarscience.msfc.nasa.gov/interior.shtml>.
- [8]NASA, <https://nssdc.gsfc.nasa.gov/planetary/factsheet/marsfact.html>.
- [9]B. Ryden *Introduction to Cosmology*, Cambridge University Press, 2019, 2nd edition.
- [10]D. Valencia, D. D. Sasselov, R. J. O'Connell, Radius and structure models of the first super-earth planet, *The Astrophysical Journal*, 656:545-551, 2007, February 10.
- [11]D. Valencia, D. D. Sasselov, R. J. O'Connell, Detailed models of super-earths: how well can we infer bulk properties? *The Astrophysical Journal*, 665:1413-1420, 2007 August 20.
- [12]T. Guillot, A. P. Showman, Evolution of "51Pegasus-like" planets, *Astronomy & Astrophysics*, 2002, 385, 156-165, DOI: 10.1051/0004-6361:20011624
- [13]T. Guillot, A. P. Showman, Atmospheric circulation and tides of "51Pegasus-like" planets, *Astronomy & Astrophysics*, 2002, 385, 166-180, DOI: 10.1051/0004-6361:20020101
- [14]L.N. Fletcher, Y. Kaspi, T. Guillot, A.P. Showman, How Well Do We Understand the Belt/Zone Circulation of Giant Planet Atmospheres? *Space Sci Rev*, 2020, 216:30. <https://doi.org/10.1007/s11214-019-0631-9>
- [15]Y. Kaspi, E. Galanti, A.P. Showman, D. J. Stevenson, T. Guillot, L. Iess, S.J. Bolton, Comparison of the Deep Atmospheric Dynamics of Jupiter and Saturn in Light of the Juno and Cassini Gravity Measurements, *Space Sci Rev*, 2020, 216:84. <https://doi.org/10.1007/s11214-020-00705-7>
- [16]Orbital Debris Program Office, *HISTORY OF ON-ORBIT SATELLITE FRAGMENTATIONS*, National Aeronautics and Space Administration, 2018, 15 th Edition.
- [17]M. Mulrooney, The NASA Liquid Mirror Telescope, *Orbital Debris Quarterly News*, 2007, April, v11i2,
- [18]Orbital Debris Program Office, Chinese Anti-satellite Test Creates Most Severe Orbital Debris Cloud in History, *Orbital Debris Quarterly News*, 2007, April, v11i2,
- [19]A. MANIS, M. MATNEY, A. VAVRIN, D. GATES, J. SEAGO, P. ANZ-MEADOR, Comparison of the NASA ORDEM 3.1 and ESA MASTER-8 Models, *Orbital Debris Quarterly News*, 2021, Sept, v25i3.
- [20]D. Wright, Space debris, *Physics today*, 2007, 10, 35-40.
- [21]TANG Zhi-mei, DING Zong-hua, DAI Lian-dong, WU Jian, XU Zheng-wen, "The Statistics Analysis of Space Debris in Beam Parking Model in 78° North Latitude Regions," *Space Debris Research*, 2017, 17, 3, 1-7.
- [22]TANG Zhimei DING, Zonghua, YANG Song, DAI Liandong, XU Zhengwen, WU Jian The statistics analysis of space debris in beam parking model based on the Arctic 500 MHz incoherent scattering radar, *CHINESE JOURNAL OF RADIO SCIENCE*, 2018, 25, 5, 537-542
- [23]TANG Zhimei, DING, Zonghua, DAI Liandong, WU Jian, XU Zhengwen, Comparative analysis of space debris gaze detection based on the two incoherent scattering radars located at 69N and 78N, *Chin . J . Space Sci*, 2018 38, 1, 73-78. DOI:10.11728/cjss2018.01.073
- [24]DING Zong-hua, YANG Song, JIANG hai, DAI Lian-dong, TANG Zhi-mei, XU Zheng-wen, WU Jian, The Data Analysis of the Space Debris Observation by the Qujing Incoherent Scatter Radar, *Space Debris Research*, 2018, 18, 1, 12-19.
- [25]YANG Song, DING Zonghua, Xu Zhengwen, WU Jian, Statistical analysis on the space posture, distribution, and scattering characteristic of debris by incoherent scattering radar in Qujing, *Chinese Journal of Radio science*, 2018 33, 6 648-654, DOI:10.13443/j.cjors.2017112301
- [26]Clet Lab, Clet: a C compiler, <https://drive.google.com/file/d/1OjKqANcgZ-9V56rgcoMtOu9w4rP49sgN/view?usp=sharing>
- [27]Huaiyang Cui, Relativistic Matter Wave and Its Explanation to Superconductivity: Based on the Equality Principle, *Modern Physics*, 10, 3(2020)35-52. <https://doi.org/10.12677/MP.2020.103005>
- [28]Huaiyang Cui, Relativistic Matter Wave and Quantum Computer, Amazon Kindle eBook, 2021.
- [29]Huaiyang Cui, Ultimate Acceleration to Calculate Atomic Spin, *viXra:2209.0041*, 2022.
- [30]Huaiyang Cui, Study of Earthquakes in Japanese Islands Using Quantum Gravity Theory with Ultimate Acceleration, *viXra:2209.0149*, 2022.
- [31]N.Cox, *Allen's Astrophysical Quantities*, Springer-Verlag, 2001, 4th ed..
- [32] S. E. Schneider, T. T. Arny, *Pathways to Astronomy*, McGraw-Hill Education, 2018, 5th ed.
- [33] https://en.wikipedia.org/wiki/E1_Ni%C3%B1o%E2%80%93Southern_Oscillation
- [34] https://en.wikipedia.org/wiki/Atmosphere_of_Earth
- [35] Y.M.Zhu, et al, *Principle of Meteorology*, China meteorology Press, 2019. p.243.
- [36] Liping Li et al, *Introduction to Atmospheric Circulation*, 2nd edition, Science Press, 2021,
- [37] https://en.wikipedia.org/wiki/Tropical_cyclone
- [38] https://en.wikipedia.org/wiki/Tropical_cyclone_basins
- [39] <https://en.wikipedia.org/wiki/pulsar>.
- [40] L A. Lyne and F. Graham-Smith, *Pulsar Astronomy*, Fourth Edition, Cambridge University Press, 2012.
- [41] Ian Morison, *Introduction to Astronomy and Cosmology*, John Wiley & Sons, 2008.